Supporting Information

Surficial Grafting of Organoimido Moieties Enhances Capacity Performance of Oxometallic Clusters

Tushar Sanjay Jadhav,[†,‡,§] Syed Ali Abbas,[♦] Kai-Ti Chu,[†] Wen-Ti Wu,[†] Yu-Yi Hsu,[†] Gene-Hsiang Lee,[◊] Su-Ying Chien,[◊] Chih-Wei Chu,*[,♦] Ming-Hsi Chiang*[,†,‡,♠]

[†] Institute of Chemistry, Academia Sinica, Nankang, Taipei 115, Taiwan

[‡] Sustainable Chemical Science and Technology, Taiwan International Graduate Program, Academia Sinica, Nankang, Taipei 115, Taiwan

[§] Department of Applied Chemistry, National Yang Ming Chiao Tung University, Hsinchu 300, Taiwan

[♦] Research Center for Applied Sciences, Academia Sinica, Nankang, Taipei 115, Taiwan

[◊] Department of Chemistry and Instrumental Center, National Taiwan University, Taipei, 106 Taiwan

[♠] Department of Medicinal and Applied Chemistry, Kaohsiung Medical University, Kaohsiung 807, Taiwan

*To whom correspondence should be addressed: chiangmh@gate.sinica.edu.tw

Contents

Experimental

General Methods. All reactions were carried out in a three neck round bottom flask under an atmosphere of purified nitrogen. All commercially available chemicals were of ACS grade and used without further purification. $[TBA]_4[Mo_8O_{26}]$ ($TBA^+ = [N^nBu_4]^+$) and $[TBA]_2[Mo_6O_{17}(t\text{-}NCy)_2]$ (Cy = cyclohexyl) were prepared according to related procedures in the literature.[1,2] Solvents were of HPLC grade and purified as follows: acetonitrile (MeCN) was distilled first over CaH_2 and then from P_2O_5 under N_2. Diethyl ether was distilled from sodium/benzophenone under N_2. Dichloromethane was distilled from CaH_2 under N_2. Acetone was distilled from molecular sieve 3 Å under N_2. Deuterated solvents obtained from Sigma-Aldrich were used without further purification.

Synthesis of $[TBA]_2[Mo_6O_{16}(t\text{-}NR)_2(\mu\text{-}NAr)]$ (1; R = cyclohexyl, Ar = 2,6-dichlorophenyl). To a flask charged with $[TBA]_4[Mo_8O_{26}]$ (1.00 g, 0.464 mmol), 2,6-dichloroaniline (75.2 mg, 0.464 mmol), *N*,*N'*-dicyclohexylcarbodiimide (DCC, 287 mg, 1.39 mmol) and pyridine (0.300 ml, 3.72 mmol), 10 mL of MeCN was added. After the reagents were well dissolved, the solution was heated at 85 °C for 12 hr. The resultant yellow-orange color solution was filtered to remove white precipitates of 1,3-dicyclohexylurea (DCU) and then the filtrate was dried under reduced pressure. The dried crude residue was re-dissolved in CH_2Cl_2 solution and purified by column chromatography on silica gel with acetone/CH_2Cl_2 (2:10 v/v) as eluent which gave desired product (0.120 g, 16%). Crystals of **1**•$0.5O(CH_2CH_3)_2$ for X-ray single crystallographic analysis were obtained from ether diffusion into acetone solution of the complex. IR (KBr pellet, signature bands): ν = 774 ($Mo\text{-}O_b$), 793 ($Mo^N\text{-}N_b$), 940 ($Mo\text{-}O_t$), 960 cm^{-1} ($Mo^N\text{-}N_t$). UV-vis (MeCN): λ_{max} (ε, M^{-1} cm^{-1}) = 350 (13200), 470 nm (1200). ^1H NMR (400 MHz, d_6-acetone, 300 K): δ 0.99 (t, $^3J_{HH}$ = 7.6 Hz, 24H; $[N(CH_2CH_2CH_2CH_3)_4]^+$), 1.13 (m, 8H; cyclohexyl), 1.27 (m, 4H; cyclohexyl), 1.49 (m, 20H; $[N(CH_2CH_2CH_2CH_3)_4]^+$, cyclohexyl), 1.70 (m, 4H; cyclohexyl), 1.84 (m, 16H; $[N(CH_2CH_2CH_2CH_3)_4]^+$), 3.48 (t, $^3J_{HH}$ =

8.4 Hz, 16H; [N(C*H*$_2$CH$_2$CH$_2$CH$_3$)$_4$]$^+$), 3.77 (m, 2H; *ipso-H*-cyclohexyl), 6.78 ppm (t, $^3J_{HH}$ = 8.0 Hz, 1H; Ar-*H*), 7.25 (d, $^3J_{HH}$ = 8.0 Hz, 2H; Ar-*H*). ESI-MS: m/z: 592.2 (calc. 593.00, [M – 2 TBA$^+$]$^{2-}$), 1427.7 (calc. 1428.48, [M – TBA$^+$]$^-$). Anal. Calcd (%) for $C_{50}H_{97}Cl_2Mo_6O_{16}N_5$: C, 35.94; N, 4.19; H, 5.85. Found: C, 35.65; N, 4.57; H, 5.91.

Synthesis of [TBA]$_2$[Mo$_6$O$_{16}$(t-NR)$_2$(μ-NAr)] (2; R = cyclohexyl, Ar = 4-nitrophenyl). Organoimido-functionalized polyoxomolybdate (POMo) **2** was synthesized via the similar procedures to those of POMo **1** wherein 4-nitroaniline (64.0 mg, 0.464 mmol) and DCC (203 mg, 0.982 mmol) were used instead. The yield of the desired product was 17% (0.131 g) after purification via column chromatography. Red block crystals of **2**•0.5O(CH$_2$CH$_3$)$_2$ for X-ray single crystallographic analysis were obtained from diffusion of diethyl ether into acetone solution. IR (KBr pellet, signature bands): ν = 777 (Mo-O$_b$), 803 (Mo^N-N$_b$), 940 (Mo-O$_t$), 963 cm^{-1} (Mo^N-N$_t$). UV-vis (MeCN): λ_{max} (ε, M^{-1} cm^{-1}) = 343 (16000), 447 nm (5600). ^{1}H NMR (400 MHz, d$_6$-acetone, 300 K): δ = 0.99 (t, $^3J_{HH}$ = 7.6 Hz, 24H; [N(CH$_2$CH$_2$CH$_2$C*H*$_3$)$_4$]$^+$), 1.15 (m, 4H; cyclohexyl), 1.28 (m, 4H; cyclohexyl), 1.39 (m, 4H; cyclohexyl), 1.48 (m, 20H; [N(CH$_2$CH$_2$C*H*$_2$CH$_3$)$_4$]$^+$, cyclohexyl), 1.78 (m, 4H; cyclohexyl), 1.84 (m, 16H; [N(CH$_2$C*H*$_2$CH$_2$CH$_3$)$_4$]$^+$), 3.48 (t, $^3J_{HH}$ = 8.8 Hz, 16H; [N(C*H*$_2$CH$_2$CH$_2$CH$_3$)$_4$]$^+$), 3.95 (t, 2H; *ipso-H*-cyclohexyl), 7.01 (d, $^3J_{HH}$ = 9.2 Hz, 2H; Ar-*H*), 8.16 ppm (d, $^3J_{HH}$ = 8.8 Hz, 2H; Ar-*H*). ESI-MS: m/z: 581.2 (calc. 581.06, [M – 2 TBA$^+$]$^{2-}$) and 1404.7 (calc. 1404.59, [M – TBA$^+$]$^-$). Anal. Calcd (%) for $C_{50}H_{98}Mo_6N_6O_{16}$: C, 36.46; H, 6.00; N, 5.10. Found: C, 36.29; H, 6.06; N, 4.85.

Synthesis of [TBA]$_2$[Mo$_6$O$_{16}$(t-NR)$_2$(μ-NAr)] (3; R = cyclohexyl, Ar = 4-(triflouromethyl)phenyl). Organoimido-functionalized POMo **3** was synthesized via the similar procedures to those of POMo **1** wherein 4-(trifluoromethyl)aniline (59 μL, 0.464 mmol) and DCC (203 mg, 0.982 mmol) were used instead. The yield of the desired product was 15% (0.115 g) after purification via column chromatography. IR (KBr pellet, signature bands): ν =

779 (Mo-O_b), 803 (Mo^N-N_b), 940 (Mo-O_t), 962 cm^{-1} (Mo^N-N_t). UV-vis (MeCN): λ_{max} (ε, M^{-1} cm^{-1}) = 336 (13000), 448 nm (1500). ^{1}H NMR (400 MHz, d_6-acetone, 300 K): δ = 0.99 (t, $^3J_{HH}$ = 7.6 Hz, 24H; $[N(CH_2CH_2CH_2CH_3)_4]^+$), 1.15 (m, 4H; cyclohexyl), 1.28 (m, 4H; cyclohexyl), 1.38 (m, 4H; cyclohexyl), 1.48 (m, 20H; $[N(CH_2CH_2CH_2CH_3)_4]^+$, cyclohexyl), 1.77 (m, 4H; cyclohexyl), 1.84 (m, 16H; $[N(CH_2CH_2CH_2CH_3)_4]^+$), 3.47 (t, $^3J_{HH}$ = 8.8 Hz, 16H; $[N(CH_2CH_2CH_2CH_3)_4]^+$), 3.93 (m, 2H; *ipso-H*-cyclohexyl), 6.99 (d, $^3J_{HH}$ = 8.8 Hz, 2H; Ar-*H*), 7.55 ppm (d, $^3J_{HH}$ = 8.4 Hz, 2H; Ar-*H*). ESI-MS: m/z: 592.2 (calc. 592.56, $[M – 2\ TBA^+]^{2–}$) and 1427.6 (calc. 1427.59, $[M – TBA^+]^–$). Anal. Calcd (%) for $C_{51}H_{98}F_3Mo_6N_5O_{16}$: C, 36.68; H, 5.91; N, 4.19. Found: C, 36.75; H, 5.87; N, 4.10.

Synthesis of $[TBA]_2[Mo_6O_{16}(t\text{-}NR)_2(\mu\text{-}NAr)]$ (4; R = cyclohexyl, Ar = 3,5-bis-(triflouromethyl)phenyl). Organoimido-functionalized POMo **4** was synthesized via the similar procedures to those of POMo **1** wherein 3,5-bis(trifluoromethyl)aniline (73 µL, 0.464 mmol) and DCC (203 mg, 0.982 mmol) were used instead. The yield of the desired product was 18% (0.143 g) after purification via column chromatography. Red block crystals of **4**•0.5$O(CH_2CH_3)_2$ for X-ray single crystallographic analysis were obtained from diffusion of diethyl ether into acetone solution. IR (KBr pellet, signature bands): ν = 778 (Mo-O_b), 803 (Mo^N-N_b), 941 (Mo-O_t), 963 cm^{-1} (Mo^N-N_t). UV-vis (MeCN): λ_{max} (ε, M^{-1} cm^{-1}) = 334 (15000), 448 nm (1500). ^{1}H NMR (500 MHz, d_6-acetone, 297.1 K): δ = 0.99 (t, $^3J_{HH}$ = 7.5 Hz, 24H; $[N(CH_2CH_2CH_2CH_3)_4]^+$), 1.14 (m, 4H; cyclohexyl), 1.30 (m, 8H; cyclohexyl), 1.49 (m, 20H; $[N(CH_2CH_2CH_2CH_3)_4]^+$, cyclohexyl), 1.76 (m, 4H; cyclohexyl), 1.84 (m, 16H; $[N(CH_2CH_2CH_2CH_3)_4]^+$), 3.47 (t, $^3J_{HH}$ = 8.5 Hz, 16H; $[N(CH_2CH_2CH_2CH_3)_4]^+$), 3.89 (m, 2H; *ipso-H*-cyclohexyl), 7.40 (s, 2H; Ar-*H*), 7.41 ppm (s, 1H; Ar-*H*). ESI-MS: m/z: 626.2 (calc. 626.56, $[M – 2\ TBA^+]^{2–}$) and 1495.7 (calc. 1495.59, $[M – TBA^+]^–$). Anal. Calcd (%) for $C_{52}H_{97}Mo_6F_6N_5O_{16}$: C, 35.93; H, 5.63; N, 4.03. Found: C, 36.11; H, 5.56; N, 3.71.

Crystallographic results

Table S1. X-ray crystallographic data of **1**, **2** and **4**.

	1	**2**	**4**
Empirical formula	$C_{52}H_{102}Cl_2Mo_6N_5O_{16.5}$	$C_{52}H_{103}Mo_6N_6O_{18.5}$	$C_{54}H_{102}F_6Mo_6N_5O_{16.5}$
Formula weight	1707.92	1684.04	1775.04
T, K	150 (2)	150 (2)	150 (2)
Crystal system	Triclinic	Monoclinic	Triclinic
Space group	P-1	$P2_1/c$	P-1
a, Å	16.5251(4)	24.5526(7)	12.3882(4)
b, Å	17.7115(4)	18.3498(5)	23.0920(7)
c, Å	24.5234(6)	15.2939(5)	27.7838(8)
α, °	71.8079(6)	90	113.2757(6)
β, °	89.1477(7)	103.8086(7)	98.5545(6)
γ, °	86.6843(7)	90	96.7016(6)
V, $Å^3$	6807.4(3)	6691.3(3)	7084.0(4)
Z	4	4	4
ρ_{calcd}, Mg m^{-3}	1.666	1.672	1.664
μ, mm^{-1}	1.213	1.159	1.108
F (000)	3468	3428	3596
Reflections collected	50054	39891	55342
Independent reflections	25302	15327	29355
R_{int}	0.0270	0.0377	0.0441
Goodness-of-fit on F^2	1.060	1.070	1.116
R1 [$I > 2\sigma(I)$] (all data)[a]	0.0483 (0.0639)	0.0444 (0.0526)	0.0642 (0.0852)
wR2 [$I > 2\sigma(I)$] (all data)[b]	0.1228 (0.1373)	0.1112 (0.1182)	0.1320 (0.1404)

[a] $R1 = (\Sigma||F_o|-|F_c||)/(\Sigma|F_o|)$. [b] $wR2 = [\Sigma w(F_o^2-F_c^2)^2/\Sigma w(F_o^2)^2]^{1/2}$.

Table S2. Selected bond distances (Å) and angles (°) of **1**, **2** and **4**.

	1	**2**	**4**
Mo^N-N_t	ave.1.713(10)	ave. 1.710(8)	ave. 1.716(6)
Mo^N-N_b	ave. 2.022(5)	ave. 2.013(4)	ave. 2.027(5)
Mo^N-O_c	ave. 2.211(3)	ave. 2.219(2)	ave. 2.216(4)
Mo-O_t	ave. 1.694(4)	ave. 1.692(3)	ave. 1.689(4)
Mo-O_c	ave. 2.379(3)	ave. 2.379(2)	ave. 2.380(4)
Mo^N-N-C	ave. 175.8(17)	ave. 172.9(8)	ave. 170.4(5)
$Mo^N N_b$-Mo^N	107.3(2)	108.01(15)	106.7(2)

Characterization

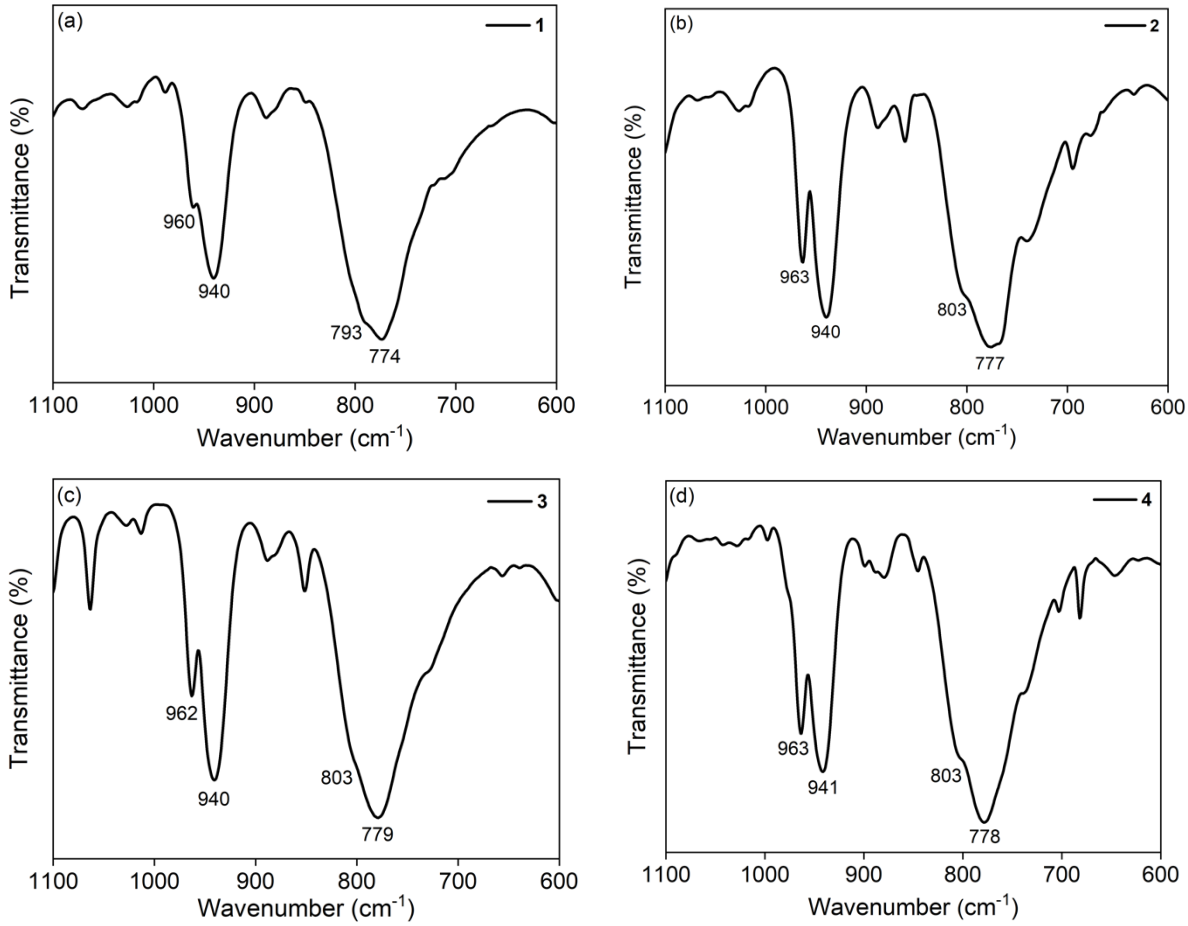

Figure S1. FTIR spectra of **1** (a), **2** (b), **3** (c) and **4** (d) in KBr pellets.

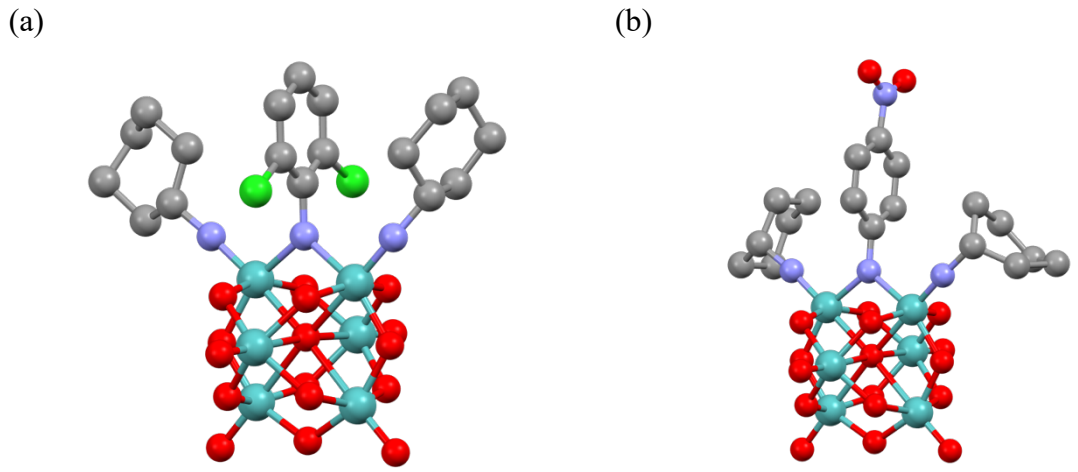

Figure S2. Molecular structures of **1** (a) and **2** (b). All hydrogen atoms are omitted for clarity. The complex is displayed as a ball-and-stick presentation. Color scheme: Mo (aqua), O (red), N (blue), C (grey) and Cl (green).

(a)

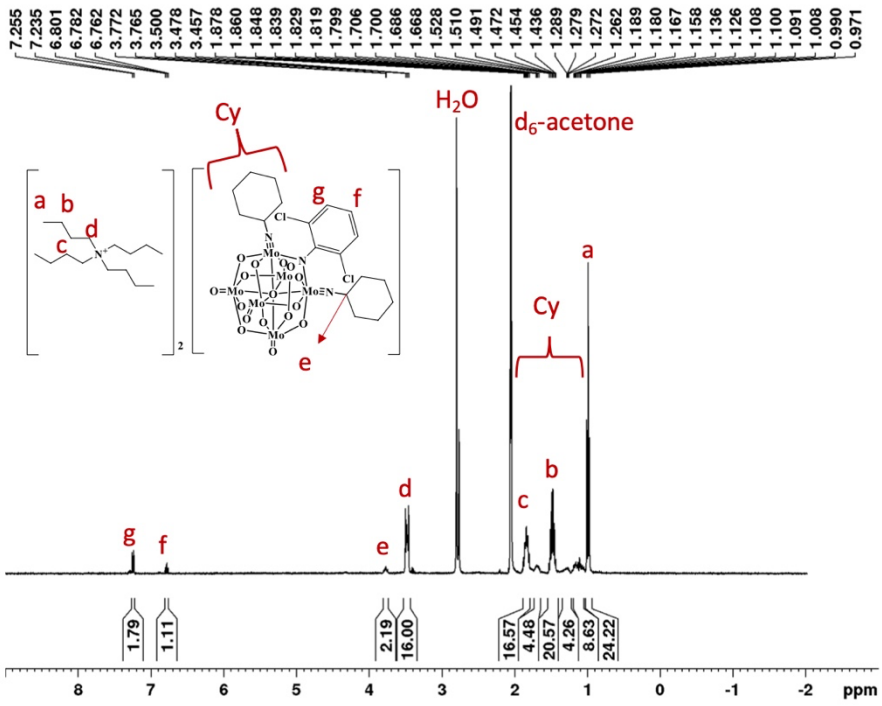
7.255
7.235
6.801
6.782
6.762
3.772
3.765
3.500
3.478
3.457
1.878
1.860
1.848
1.839
1.829
1.819
1.799
1.706
1.700
1.686
1.668
1.528
1.510
1.491
1.472
1.454
1.436
1.289
1.279
1.272
1.262
1.189
1.180
1.167
1.158
1.136
1.126
1.108
1.100
1.091
1.008
0.990
0.971
Cy
H2O
d6-acetone
a b
c
d
g f
e
a
Cy
b
c
d
g
f
e
1.79
1.11
2.19
16.00
16.57
4.48
20.57
4.26
8.63
24.22
8 7 6 5 4 3 2 1 0 -1 -2 ppm

(b)

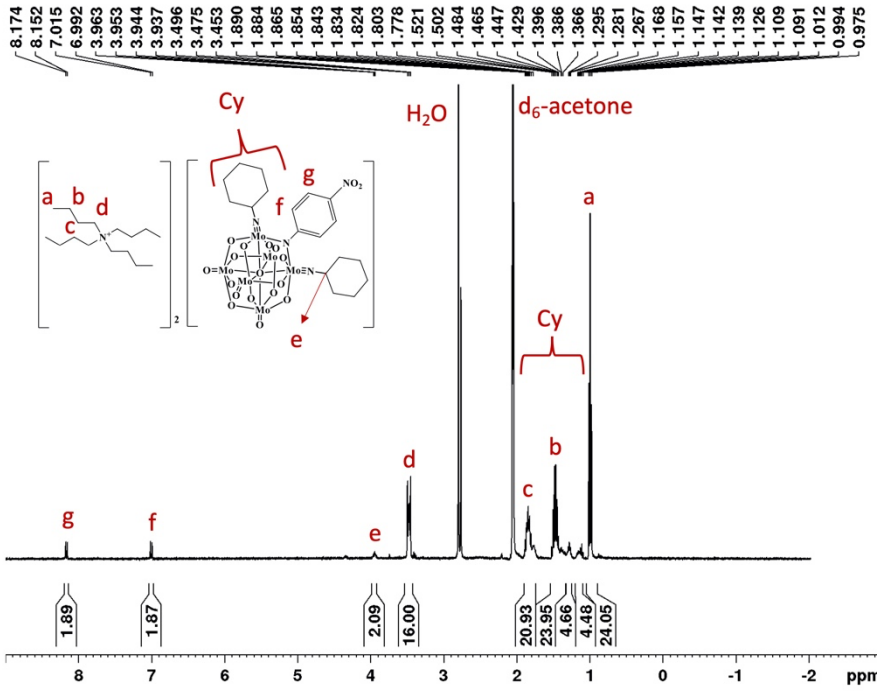
8.174
8.152
7.015
6.992
3.963
3.953
3.944
3.937
3.496
3.475
3.453
1.890
1.884
1.865
1.854
1.843
1.834
1.824
1.803
1.778
1.521
1.502
1.484
1.465
1.447
1.429
1.396
1.386
1.366
1.295
1.281
1.267
1.168
1.157
1.147
1.142
1.139
1.126
1.109
1.091
1.012
0.994
0.975
Cy
H2O
d6-acetone
a b
c
d
g
f
NO2
e
a
Cy
b
c
d
g
f
e
1.89
1.87
2.09
16.00
20.93
23.95
4.66
4.48
24.05
8 7 6 5 4 3 2 1 0 -1 -2 ppm

(c)

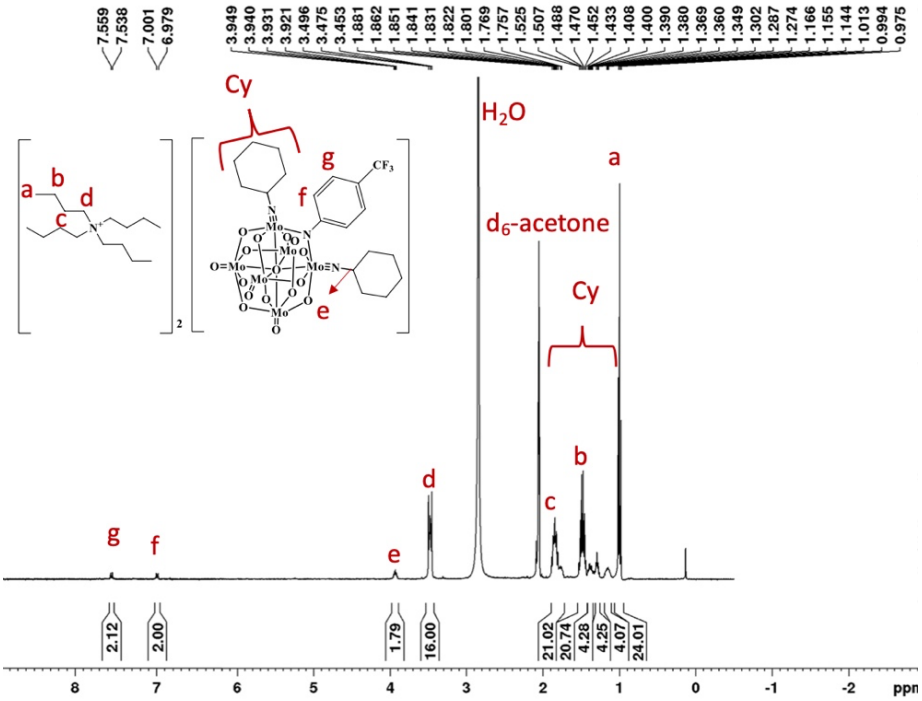

(d)

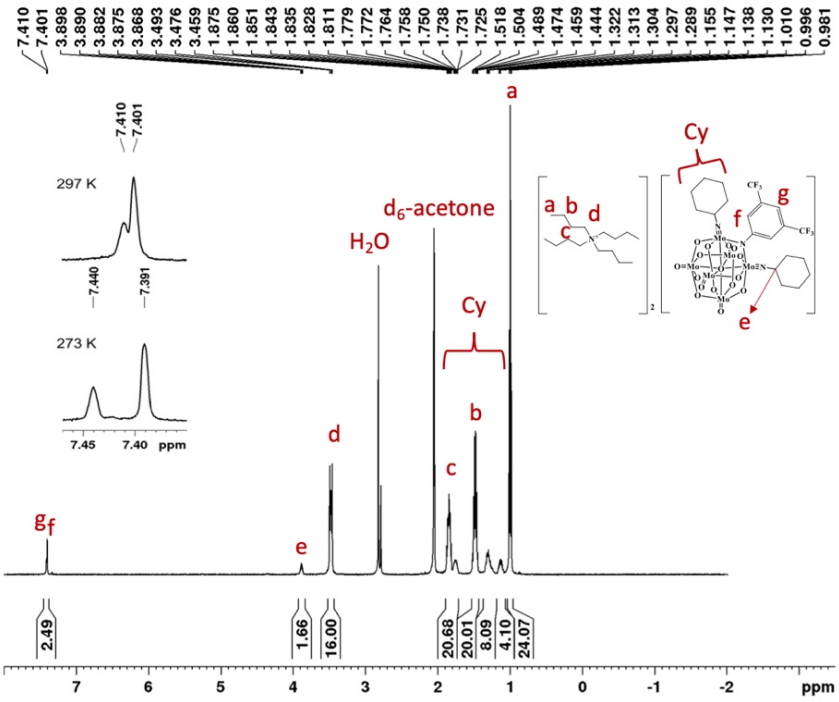

Figure S3. ^{1}H-NMR spectra of **1** (a), **2** (b), **3** (c) and **4** (d) in d_6-acetone solution.

(a)

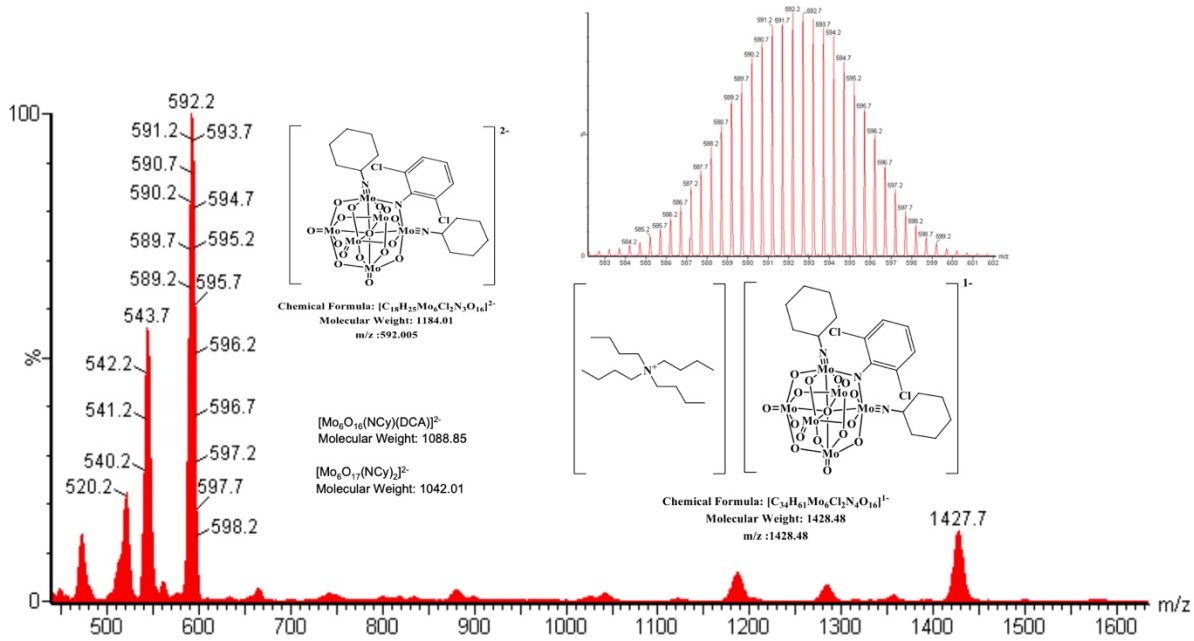
100
%
0
592.2
591.2
593.7
590.7
590.2
594.7
589.7
595.2
589.2
595.7
543.7
596.2
542.2
541.2
596.7
540.2
597.2
520.2
597.7
598.2
1427.7
Chemical Formula: [C18H25Mo6Cl2N3O16]2-
Molecular Weight: 1184.01
m/z :592.005
[Mo6O16(NCy)(DCA)]2-
Molecular Weight: 1088.85
[Mo6O17(NCy)2]2-
Molecular Weight: 1042.01
Chemical Formula: [C34H61Mo6Cl2N4O16]1-
Molecular Weight: 1428.48
m/z :1428.48
500
600
700
800
900
1000
1100
1200
1300
1400
1500
1600
m/z

(b)

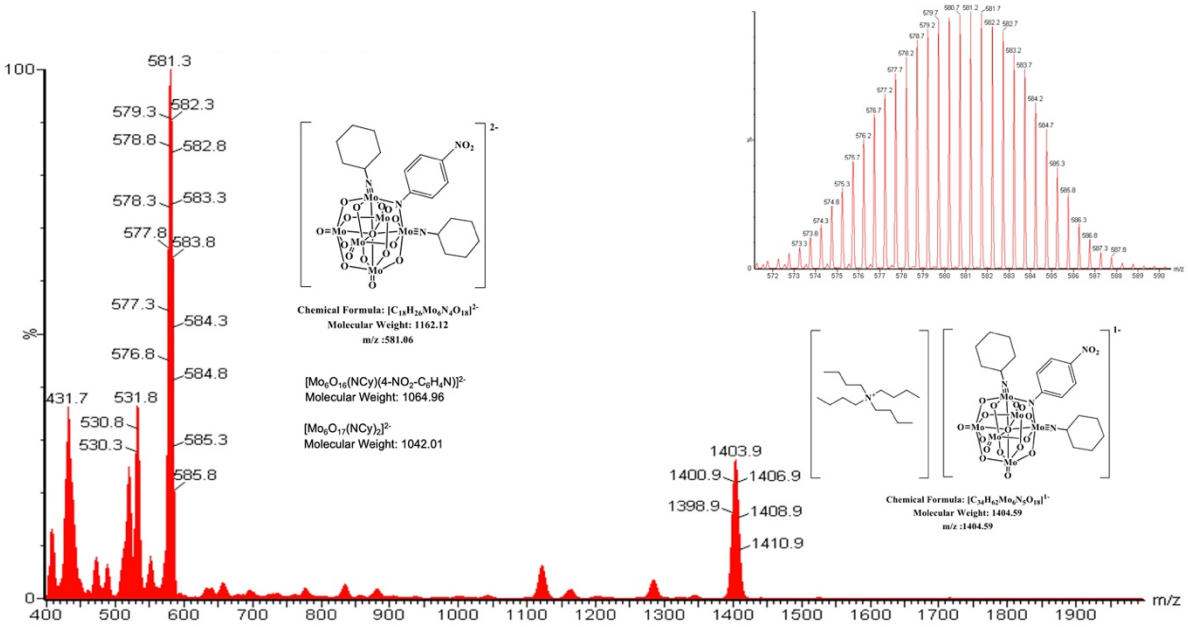
100
%
0
581.3
579.3
582.3
578.8
582.8
578.3
583.3
577.8
583.8
577.3
584.3
576.8
584.8
431.7
531.8
530.8
530.3
585.3
585.8
1403.9
1400.9
1406.9
1398.9
1408.9
1410.9
Chemical Formula: [C18H26Mo6N4O18]2-
Molecular Weight: 1162.12
m/z :581.06
[Mo6O16(NCy)(4-NO2-C6H4N)]2-
Molecular Weight: 1064.96
[Mo6O17(NCy)2]2-
Molecular Weight: 1042.01
Chemical Formula: [C34H62Mo6N5O18]1-
Molecular Weight: 1404.59
m/z :1404.59
400
500
600
700
800
900
1000
1100
1200
1300
1400
1500
1600
1700
1800
1900
m/z

(c)

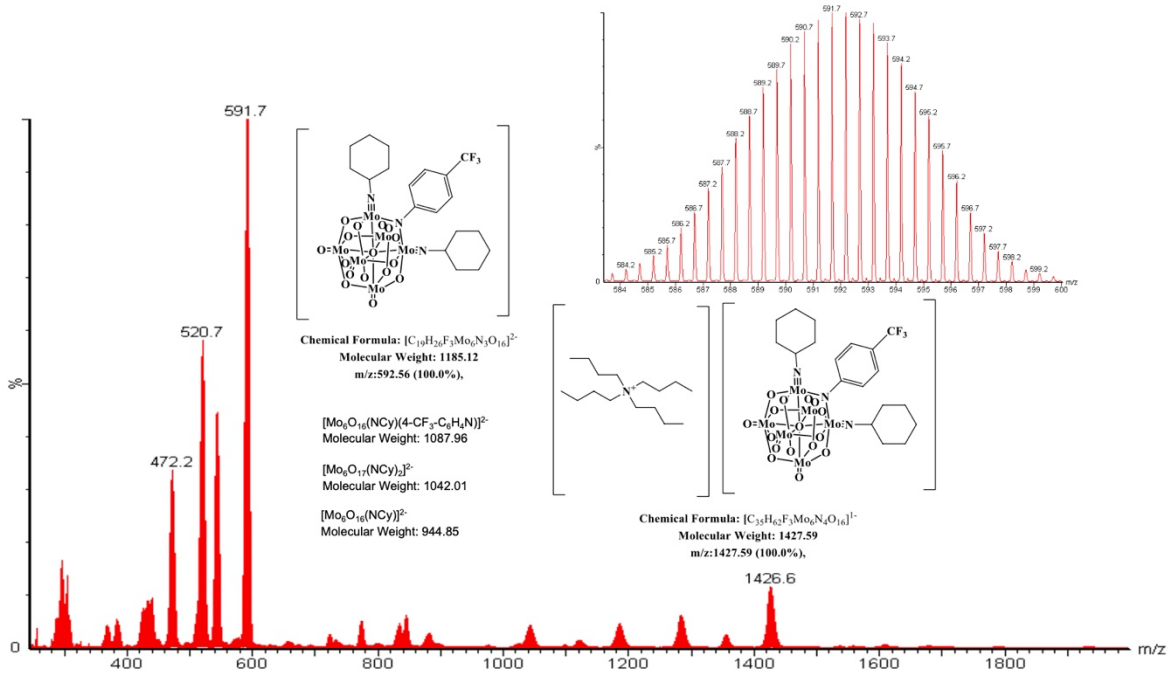

(d)

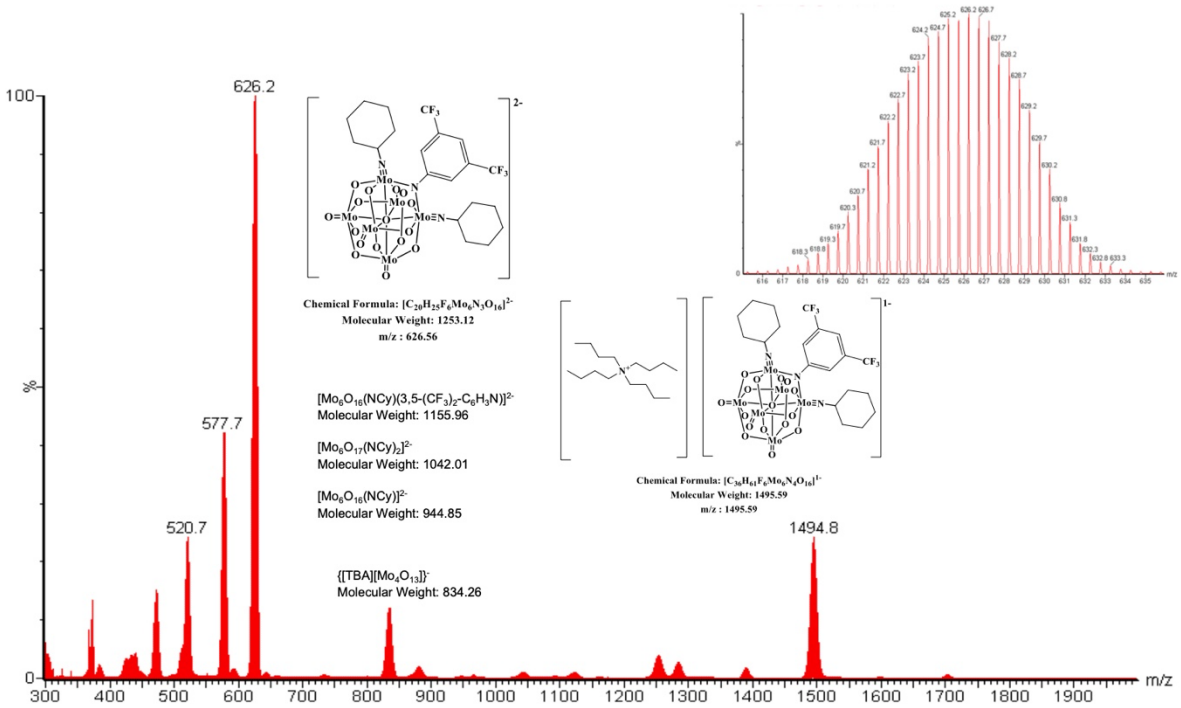

Figure S4. ESI-MS spectra of **1** (a), **2** (b), **3** (c) and **4** (d). The expanded MS patterns for the core anions are displayed.

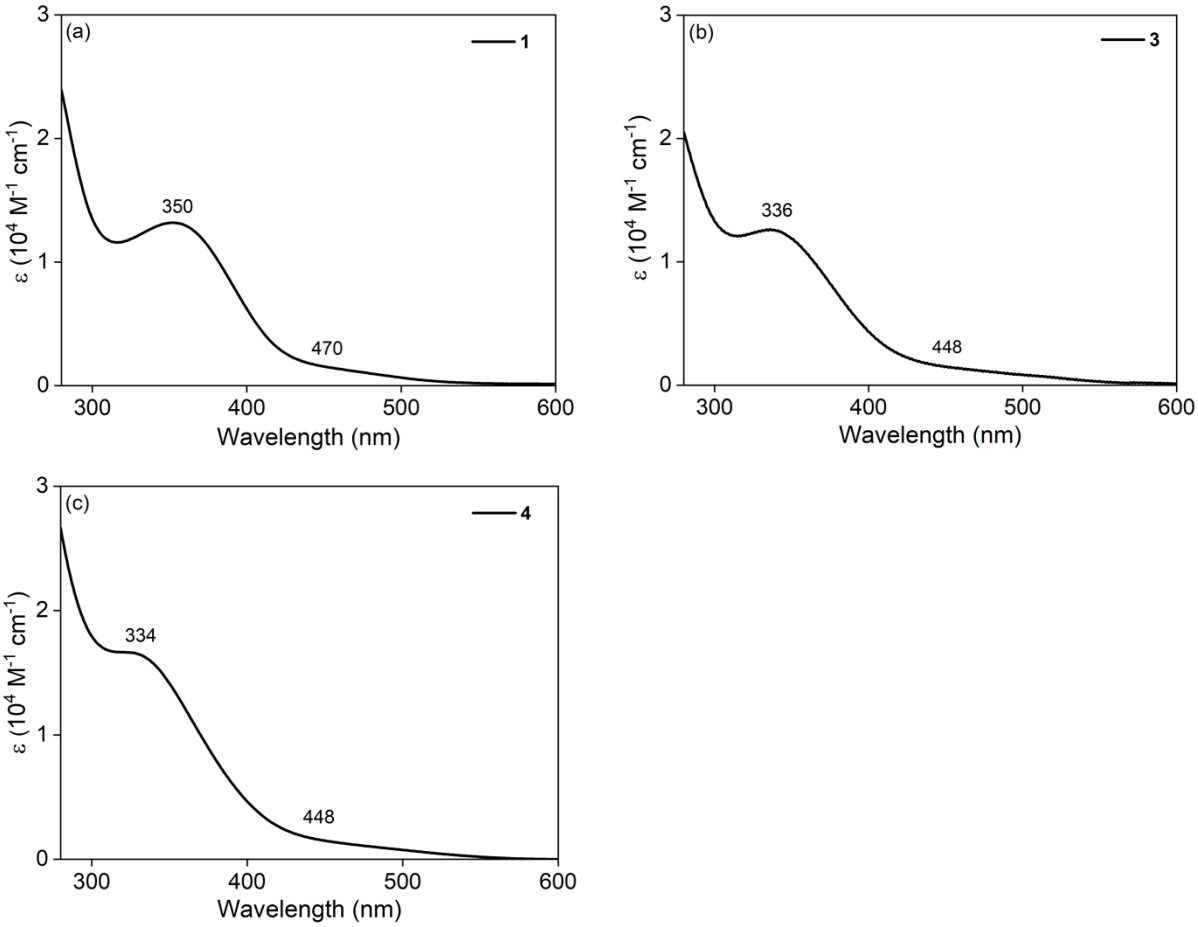

Figure S5. UV-vis spectra of **1** (a), **3** (b) and **4** (c) in MeCN solution.

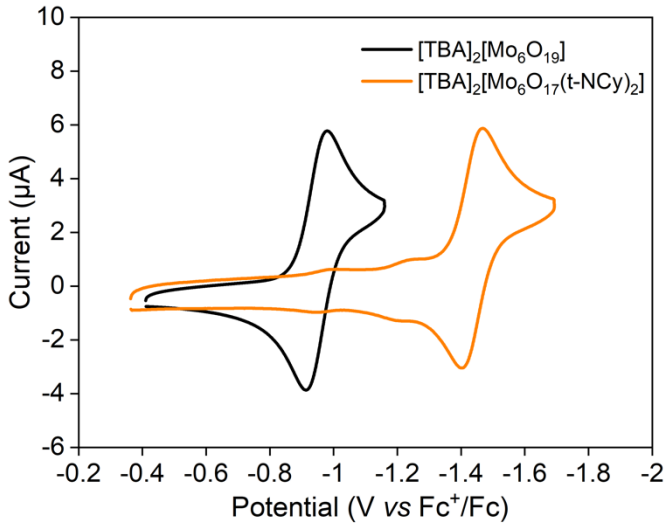

Figure S6. Comparison of cyclic voltammograms of $[TBA]_2[Mo_6O_{19}]$ and $[TBA]_2[Mo_6O_{17}(t\text{-}NCy)_2]$ in acetone solution (0.25 mM, $\upsilon = 0.1$ V s^{-1}, 1 mm vitreous carbon electrode, 298 K).

(a)

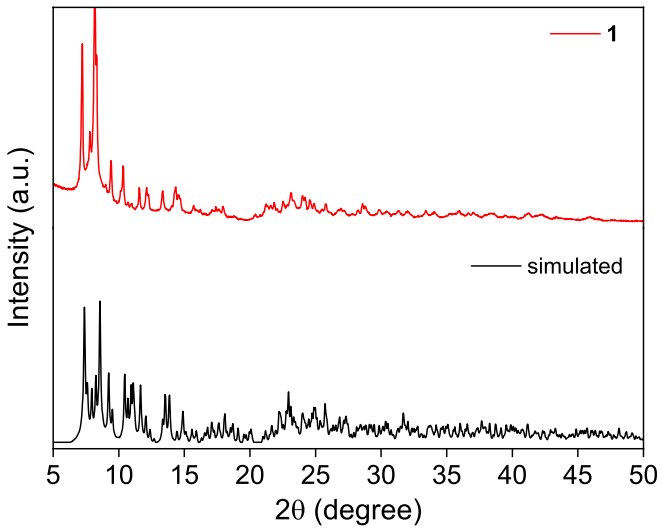
1
simulated
Intensity (a.u.)
5
10
15
20
25
30
35
40
45
50
2θ (degree)

(b)

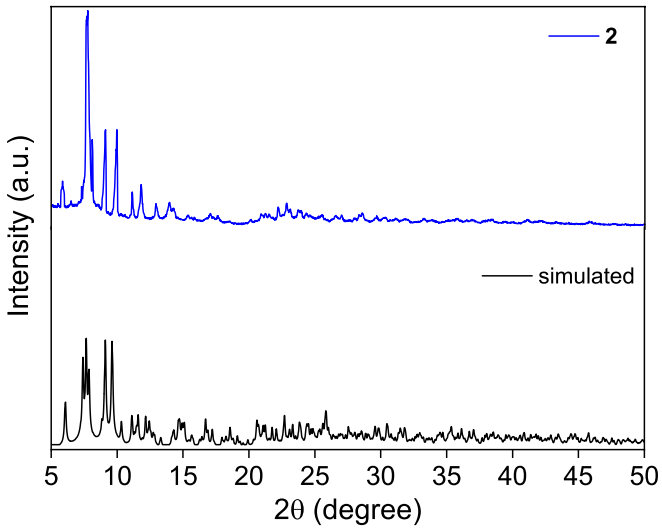
2
simulated
Intensity (a.u.)
5
10
15
20
25
30
35
40
45
50
2θ (degree)

(c)

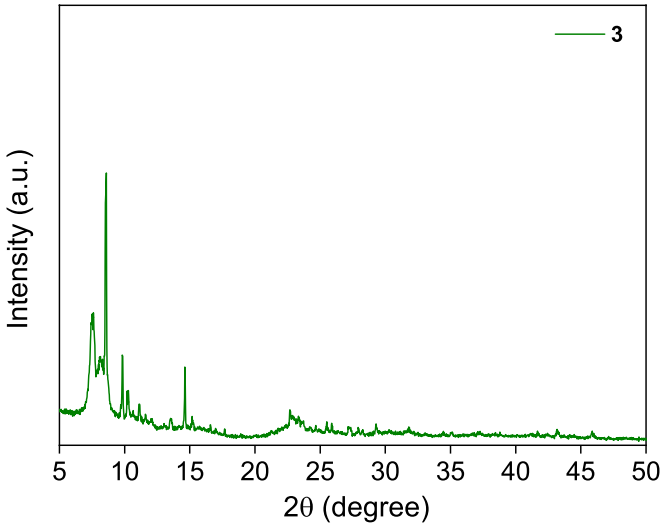
3
Intensity (a.u.)
5
10
15
20
25
30
35
40
45
50
2θ (degree)

(d)

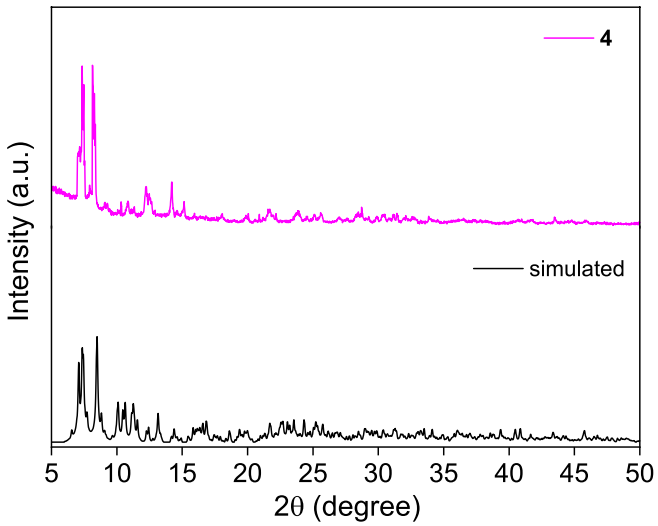

Figure S7. pXRD spectra of **1** (a), **2** (b), **3** (c) and **4** (d).

Thermal stability of the organoimido-functionalized POMos

The organoimido-functionalized POMos remain stable in the process of the electrode preparation. Thermal degradation of POMos **1-4** was investigated by thermogravimetric analysis (TGA). The thermal behavior of **1-4** in the lower temperature region is a 2-step gradual process. The weight loss up to 2% < 200 °C accounts for the loss of solvent molecules. Dissociation of the organic components including the organoimido and cyclohexyl groups occurs at higher temperatures around 200-300 °C. The thermal decomposition of $[TBA]^+$ cations accounts for the descending process in 300-400 °C. Starting 450 °C, the $\{Mo_6O_{19-x}\}$ fragments of all samples are decomposed to metal-oxide greenish-black residues, which are confirmed to be MoO_3 according to pXRD patterns. According to the TGA results, it is concluded that all complexes remain intact in the fabrication process to coin cells for the capacity measurements.

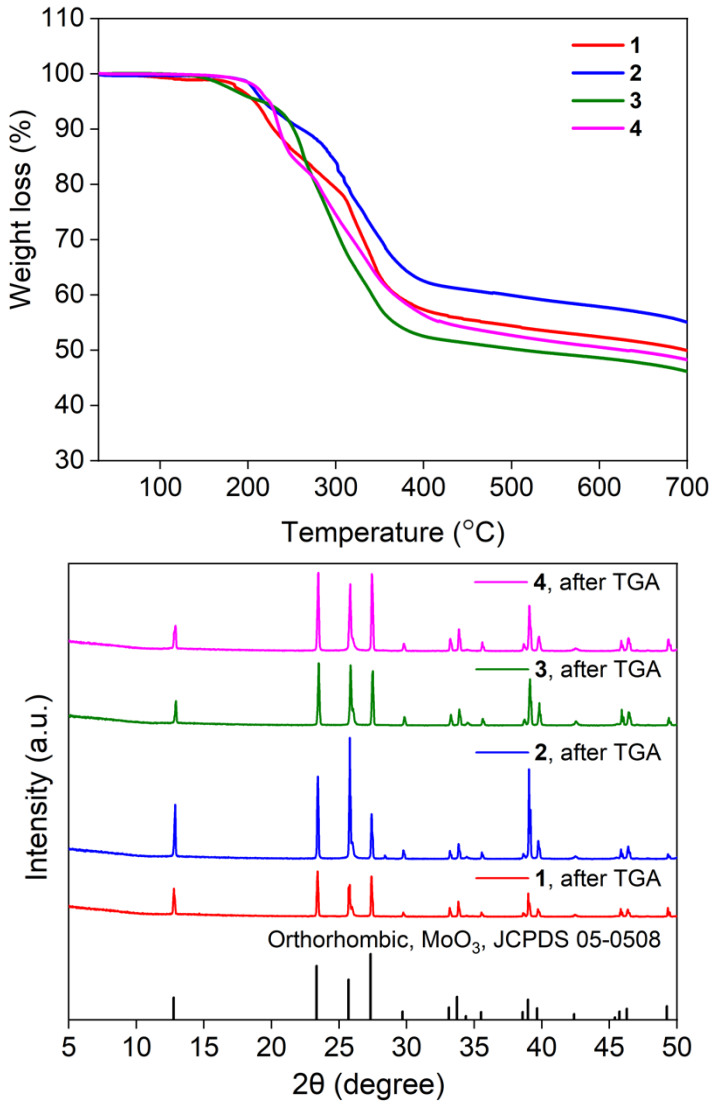

Figure S8. TGA plots of **1-4** (upper) and the pXRD patterns of the samples after TGA measurements (bottom).

EIS measurements and fits

Nyquist plots of the electrode materials composed of **1-4** at an amplitude of 5 mV are shown in the main text. The corresponding results of $[TBA]_2[Mo_6O_{19}]$ and $[TBA]_2[Mo_6O_{17}(t\text{-}NCy)_2]$ are also displayed in the following figure for comparison. The equivalent circuit model shown below is used to evaluate the internal resistance of the tested cells. The simulated results are summarized in the table in which the parameters R_s, R_{ct}, CPE_{ps}, CPE_{dl} and W1 are the electrolyte resistance, the interfacial charge transfer resistance, constant phase elements representing the pseudo-capacitance of the electrode material, and the capacitance of the double-layer at the electrode surface, and Warburg term, respectively.

(a)

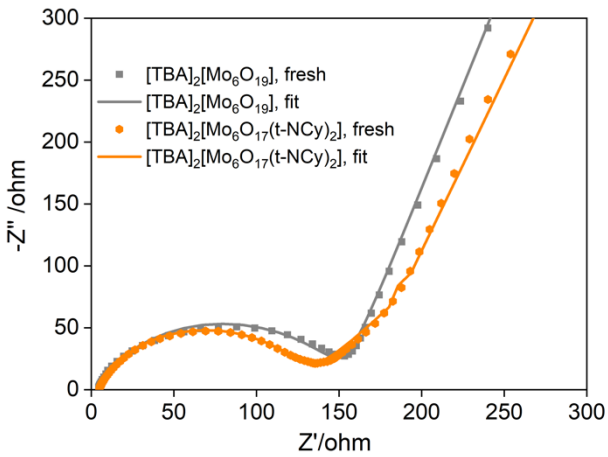

(b)

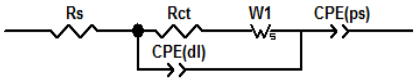

Complex	R_s (Ω)	R_{ct} (Ω)	CPE_{ps} (mF)	CPE_{dl} (μF)	W1 (Ω)
1	3.14	79.4	2.71	9.68	1347
2	2.58	89.4	5.21	15.3	2797
3	4.53	80.2	4.44	16.5	1394
4	3.63	100.9	9.87	10.4	382
$[TBA]_2[Mo_6O_{17}(t\text{-}NCy)_2]$	4.46	134.0	2.81	14.8	2522
$[TBA]_2[Mo_6O_{19}]$	3.56	146.8	1.44	12.3	2110

Figure S9. Nyquist plots of the electrode materials composed of $[TBA]_2[Mo_6O_{19}]$ and $[TBA]_2[Mo_6O_{17}(t\text{-}NCy)_2]$ at an amplitude of 5 mV (a). Equivalent circuit model of the electrode/electrolyte interface for the electrode material (b). The table summarizes the best results fitted to the model.

Surface areas and porosity

The N_2 adsorption-desorption isotherms of **1-4** are classified to type IV isotherm, suggesting the materials with various porosity ranging from micro to meso sizes. The low-pressure isotherms exhibit negligible uptake except for **1**, suggesting adsorption in micropores. The hysteresis behavior suggests that the POMo aggregates are not rigid and dislocated in the process of adsorption/desorption. Pore swelling occurs under low pressure.

Higher surface areas and larger pore volumes of electrode materials fabricated with POMo suggest that deposition of the POMo clusters with larger steric hindrance onto CB is able to better enhance the interfacial contact with the electrolytes and increase the accumulation of Li^+ ions.

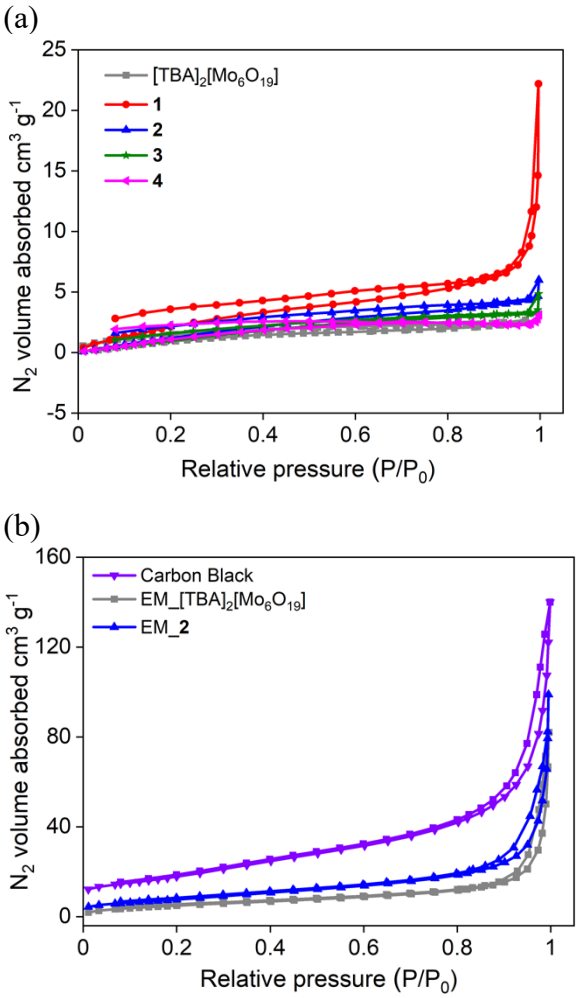

Figure S10. N_2 adsorption-desorption isotherms of **1-4** (a) and electrode materials, EM_AM (AM = **2**, $[TBA]_2[Mo_6O_{19}]$) (b).

Table S3. BET surface areas and pore volumes of **1-4**, $[TBA]_2[Mo_6O_{19}]$, $[TBA]_2[Mo_6O_{17}(t\text{-}NCy)_2]$, CB and electrode materials (EM_AM).

POMs	BET surface area ($m^2\ g^{-1}$)	Pore volume ($cm^3\ g^{-1}$)
1	10.9964	0.022615
2	8.6896	0.007203
3	7.0847	0.005421
4	8.4948	0.004289
$[TBA]_2[Mo_6O_{17}(t\text{-}NCy)_2]$	4.5887	0.006811
$[TBA]_2[Mo_6O_{19}]$[a]	4.5590	0.003568
EM_**2**	28.8089	0.126694
EM_$[TBA]_2[Mo_6O_{19}]$[a]	19.2620	0.101091
CB[a]	65.8092	0.188814

[a] The values are taken from *ACS Appl. Energy Mater.* **2021**, *4*, 643-654.

Electrochemical cycling performance

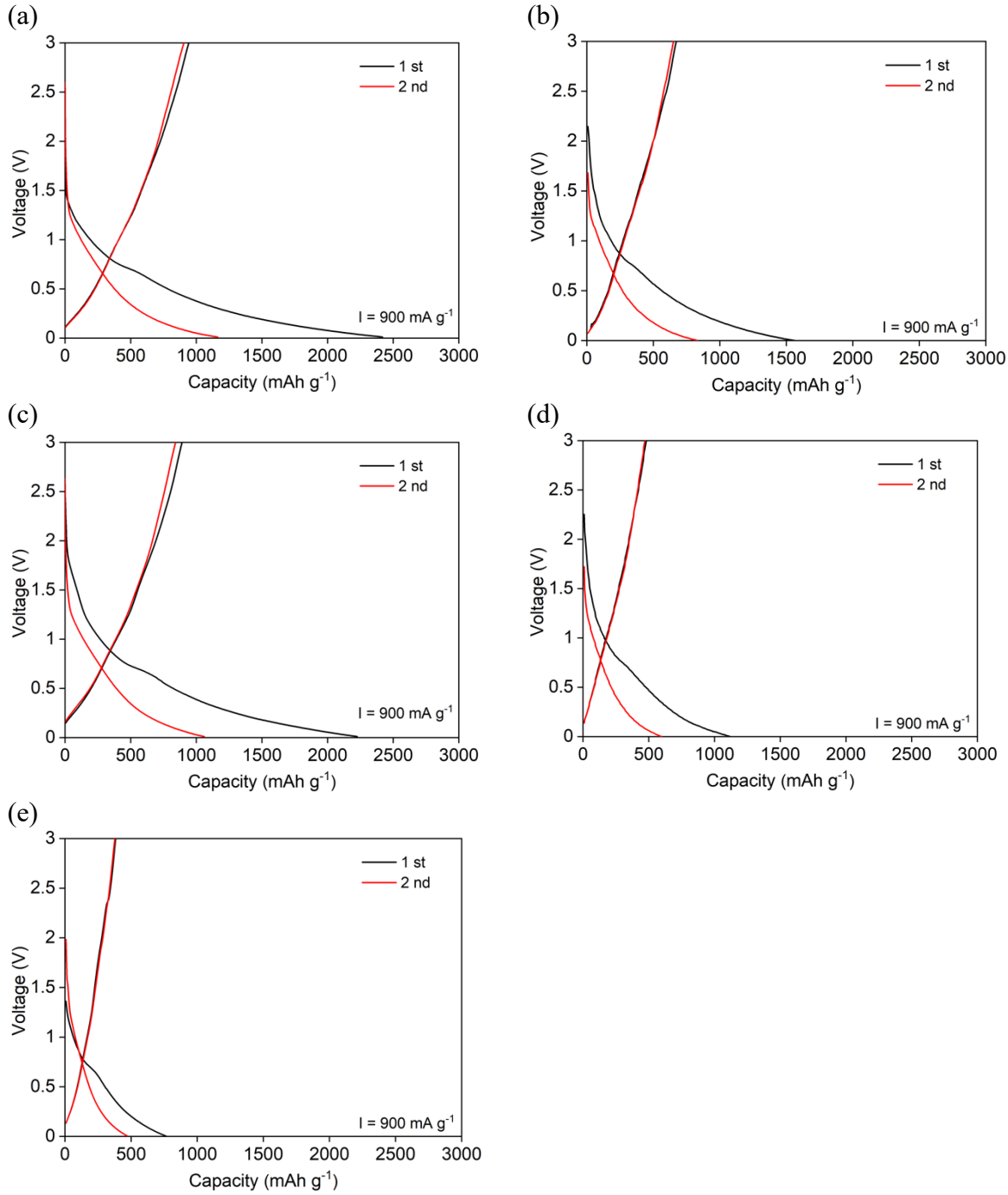

Figure S11. The 1st and 2nd charge-discharge cycle of **1** (a), **2** (b), **3** (c), **4** (d) and $[TBA]_2[Mo_6O_{19}]$ (e) at 900 mA g^{-1}.

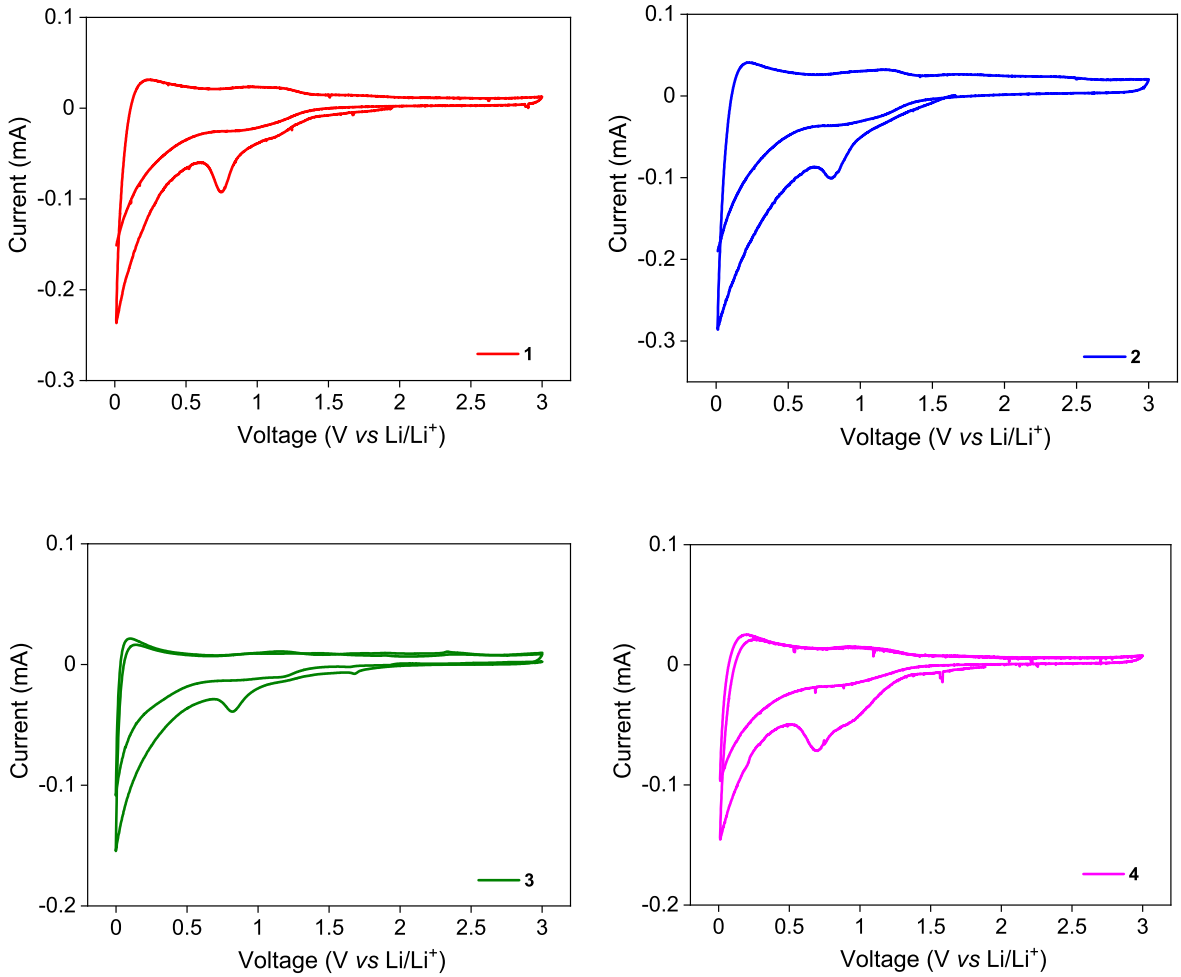

Figure S12. Cyclic voltammogram of a coin cell comprised of **1-4** in the potential range of 0-3 V vs Li/Li^+ at a scan rate of 0.05 mV s^{-1}. The irreversible reduction peak at 0.78 V is ascribed to the formation of the SEI layer. It became less obvious at the second cycle, suggesting that the stable SEI layer has formed.

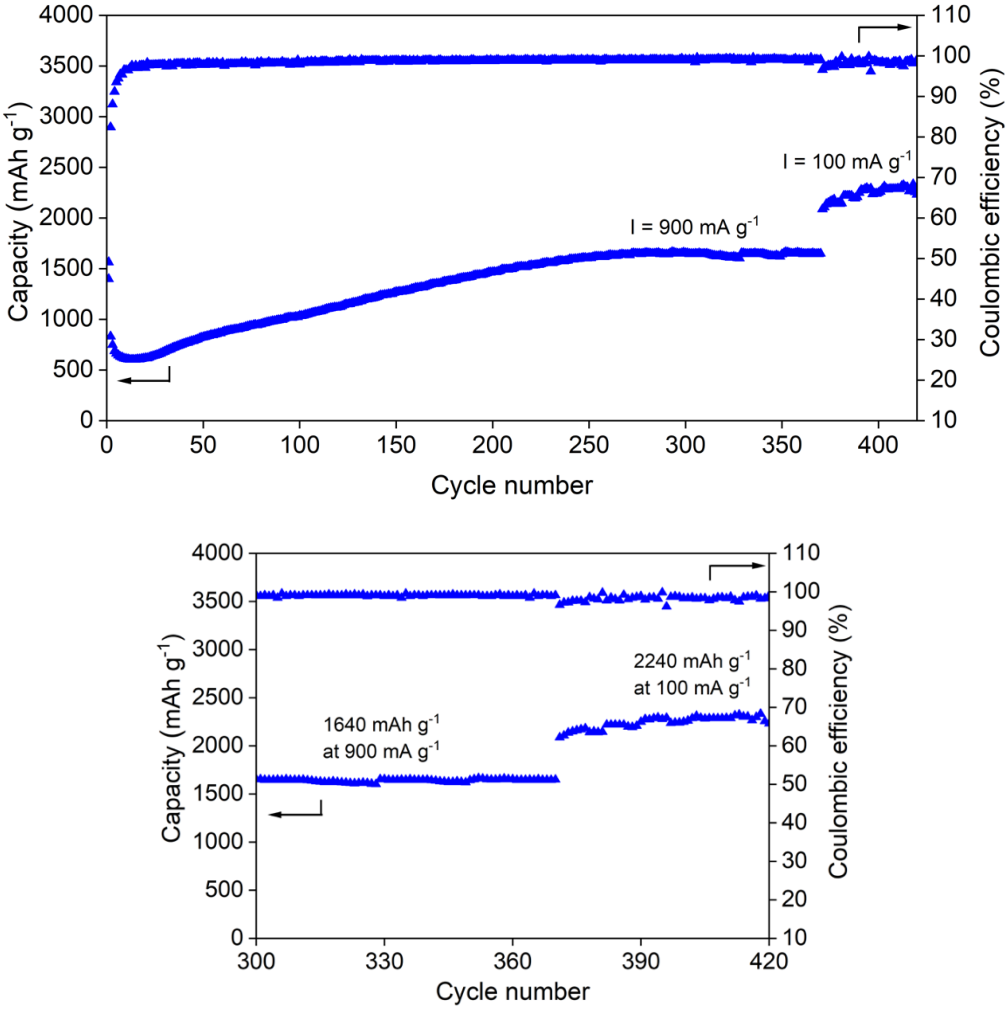

Figure S13. Cycle performance of **2** at the rate of 900 mA g^{-1} and then at 100 mA g^{-1} after the plateau is reached. The results in the expanded range are displayed in the bottom figure.

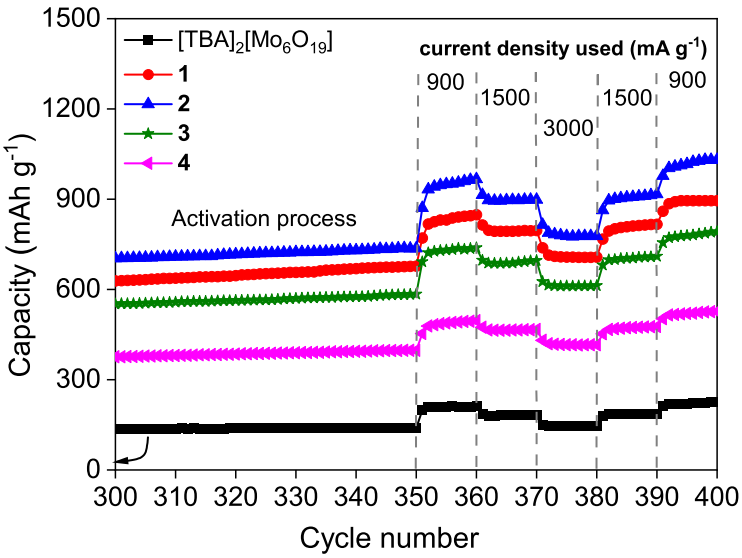

Figure S14. Rate performance and cycling stability of **1-4** at various current density between 900 and 3000 mA g^{-1}. $[TBA]_2[Mo_6O_{19}]$ is shown for comparison. For first 350 cycles, capacity performance is performed at 3000 mA g^{-1} for activation, and then rate performance and cycling stability experiment are performed at 900, 1500 and 3000 mA g^{-1} for 10 cycles each.

Surface morphology of the electrode material

Morphological changes of the electrode materials after the achievement of the plateaued capacity at the high C-rate cycles are observed in electron microscopy images. The fresh electrode material exhibited round-shaped particles (~80 nm diameter) that constitute 3-D surficial structures with numerous varied sized cavities, shown in scanning electron microscopy (SEM) images (Figure S15a). A multilayered coating with openings greater than a few μm was observed on the surface of the cycled electrode after the charge−discharge cycles (Figure S15b). The top coating possibly was a mixture of the SEI layer and the electrolyte residues. The formation of ~3 μm thick coating was clearly observed (Figure 6b). It is reported that the organic substituents on the POMo clusters exerts a significant influence on the morphology of the surficial coating, facilitating the formation of structural openings.[3] The electrolytes were removed after the cycled electrode was rinsed with THF. It exposed insoluble inorganic components on the surface of the electrode material. Without the obstruction of organically soluble substances, it is evident that agglomeration of the cluster materials occurs during the charge−discharge processes and the aggregated particles are conjectured to be bonded to larger domains that are glazed by the SEI layer (Figure S15c).

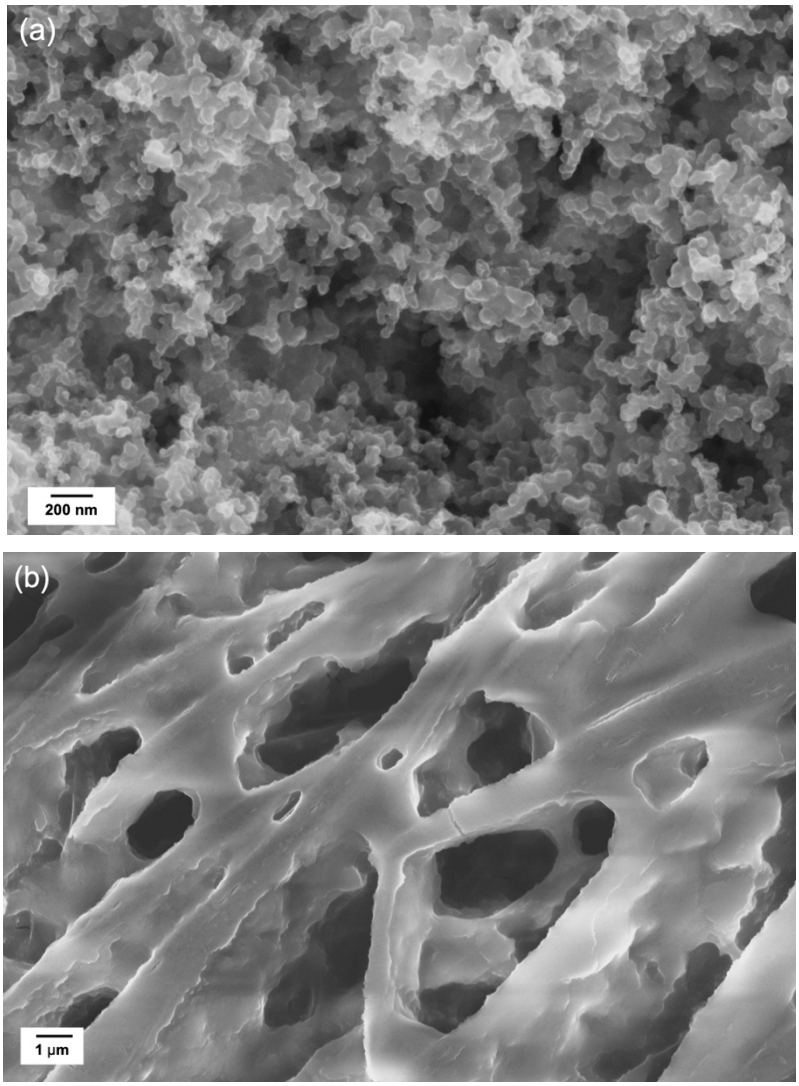

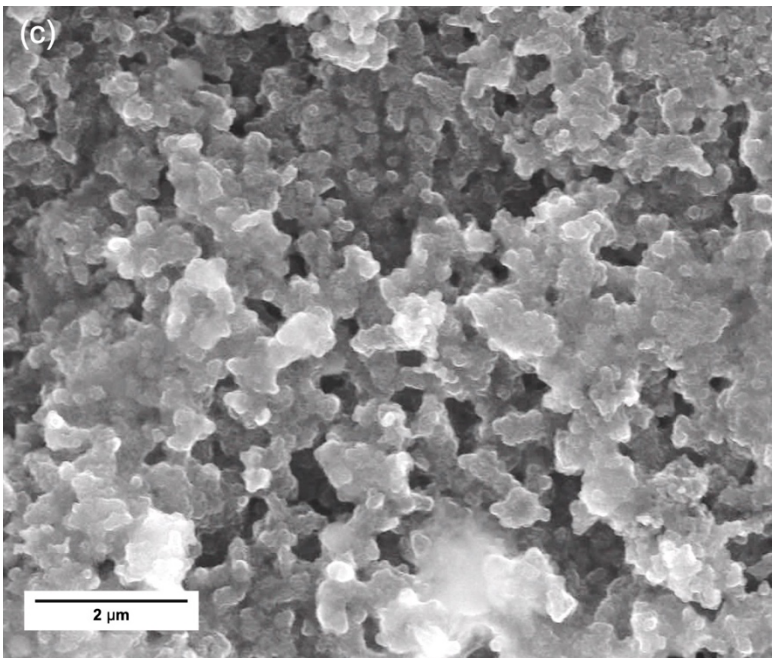

Figure S15. SEM images of the electrode materials of **2** in the freshly prepared form (a) and after the plateau is achieved (b). SEM image of the plateaued electrode after wash (c).

Investigation of stability of the plateaued electrode material POMo 2

The results of FTIR spectra suggest that the POMo **2** in the plateaued electrode material is structurally stable after the charge-discharge cycles. The coin cell comprised of electrode material POMo **2** after 1400 high C-rate charge-discharge cycles was dismantled in dry box. The anode was removed from the coin cell, and washed by the following steps: dipped in THF solution for 2-3 times and gently rinsed with THF. Next, the anode was rinsed with hexane and left on a glass plate to dryness. The dried electrode material scratched from the copper foil was ground with KBr, and pressed to pellets for the FTIR measurements. The IR profile of the cycled POMo **2** is similar to that of the fresh one while shifted to lower wavenumber by ~ 100 cm^{-1} (Figure S16). The $\nu(Mo^N\text{-}N_t)$ and $\nu(Mo\text{-}O_t)$ for the cycled POMo **2** are 865, 834 cm^{-1}, respectively. For the fresh one, they are 962, 941 cm^{-1}, respectively. The vibrational band of the $Mo\text{-}O_b$ is 672 and 773 cm, respectively, for the cycled and fresh POMo **2**. The results suggest that POMo **2** in the cycled electrode is in the reduced state, and the cluster structure stays intact.

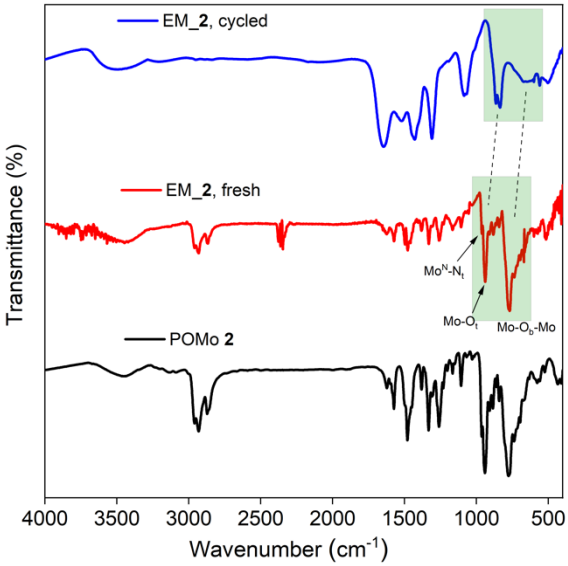

Figure S16. Comparison of FTIR spectra of POMo **2**, and the fresh electrode material comprised of POMo **2** (EM_**2**) and the cycled electrode material comprised of POMo **2** in KBr pellets.

Table S4. A list of anode materials fabricated with discrete POMs, and selected high-capacity POM composite or Mo_xO_y bulk materials for the application of lithium-ion batteries.

Material	Capacity ($mAh\ g^{-1}$)/cycles	Current Density ($mA\ g^{-1}$)	Ref
Discrete POMs			
POMo **1**	1611/360	900	
POMo **2**	1653/360	900	this
POMo **3**	1570/360	900	work
POMo **4**	1216/360	900	
	1910/450	100	
$[TBA]_2[Mo_6O_{16}(t\text{-}NCy)_2(\mu\text{-}2,6\text{-}(Me_2C_5H_2N))]$	1275/550	800	3
	840/500	900	
$Na_2K_{23}\{[(Mo^{VI})Mo^{VI}_5O_{21}(H_2O)_3(KSO_4)]_{12}[(V^{IV}O)_{30}(H_2O)_{20}(SO_4)_{0.5}]\}\bullet ca200H_2O$	1290/100	100	4
$[\{Mo_6O_{19}\}\subset\{Mo_{72}Fe_{30}O_{254}(CH_3COO)_{12}(H_2O)_{96}\}]\bullet 150H_2O$	1239/100	100	5
Mo_6O_{18}-SCN	876/100	50	6
POM composite			
HP-NENU-5/CC	1723/100	200	7
PMo_{12}-SiO_2@N-C	1641/1000	2000	8
mPMA	1517/200	500	9
$MnMo_6$-$2NH_3$-GO-2	1143/100	100	10
(PANi)-PMo_{12}/CC	1092/200	1000	11
$[CoMo_8O_{26}]_\infty$	1083/100	100	12
PMG-3	1075/100	50	13
MIL-88A@PMo_{12}	1062/100	200	14
Co-SiW@GO-30	1037/80	100	15
Co-SiW-B	1013/80	100	15
$[Co_3O(CH_3CO_2)_6(C_5H_5N)_3]^+/[PMo_{12}O_{40}]^{3-}$/SWNT	1012/100	100	16
$[PMo_8^{V}Mo_4^{VI}O_{37}(OH)_3Zn_4][BPP]_2\bullet 2[pyridine]\bullet 2H_2O$	1004/100	100	17
PMo_{12}/PANI/MWNTs	1000/100	0.5[a]	18
$[AlMo_6O_{24}H_6]^{3-}$-EDAG	1000/100	100	19
Cu-BTDB-POM@CNT	1000/300	200	20
Mo_xO_y bulk materials			
mesoporous MoO_2	0.1[b]	1607/50	21
MoO_2/MWCNTs	100	1143/200	22
MoO_2/C	500	1134/200	23
C-MoO_2/MoS_2	1000	1047/300	24
MoO_2/graphene	100	1010/60	25
MoO_3 NP[c]	0.1[b]	382/100	26

[a] $mA\ cm^{-1}$. [b] C-rate. [c] for comparison.

Computed frontier molecular orbitals and energy diagrams

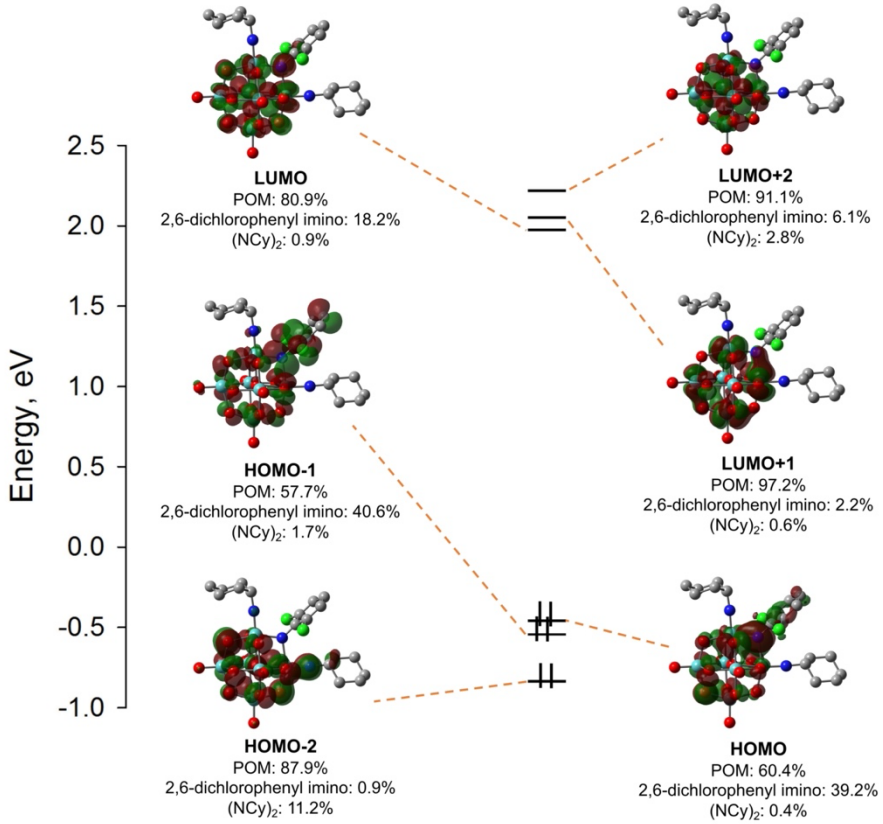

Figure S17. Energy diagram of frontier molecular orbitals for POMo **1** (isovalue = 0.03).

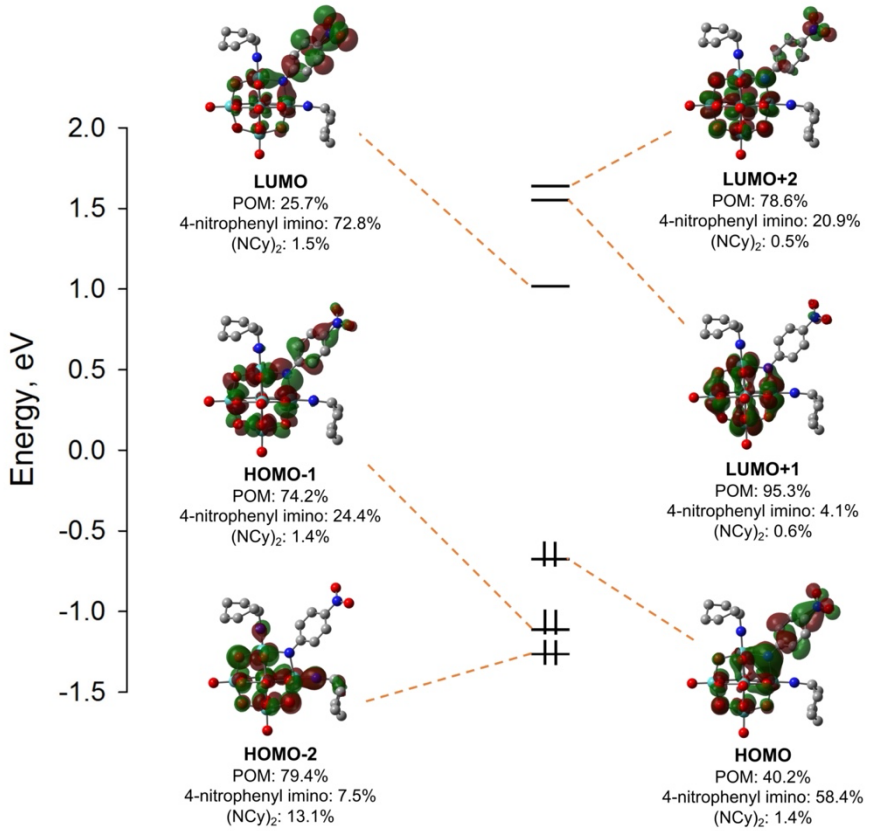

Figure S18. Energy diagram of frontier molecular orbitals for POMo **2** (isovalue = 0.03).

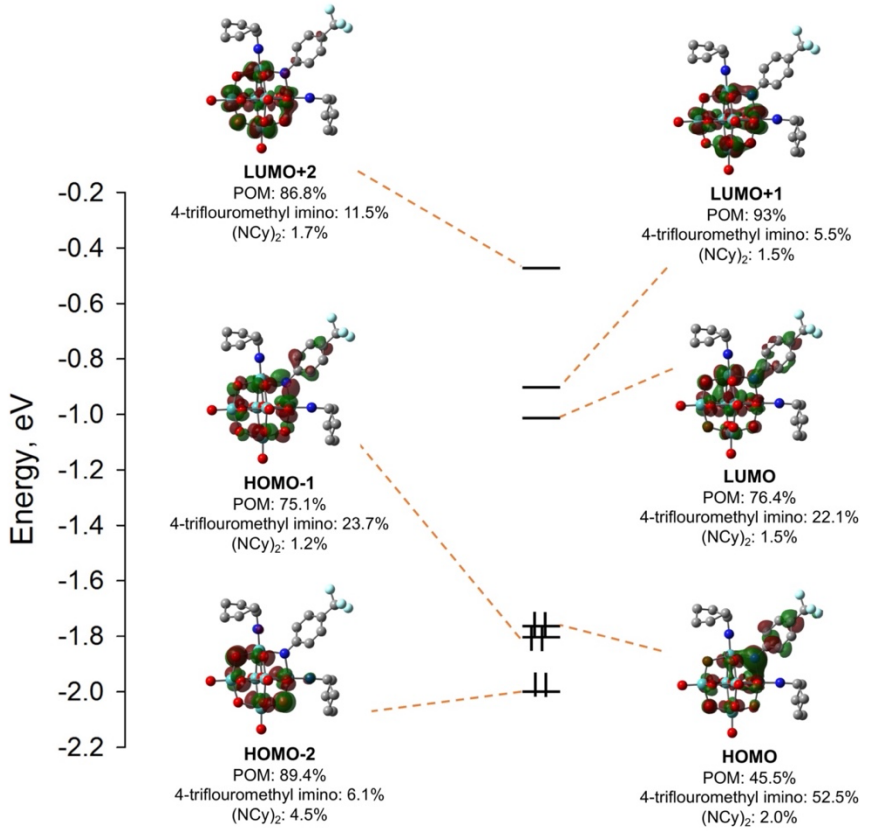

Figure S19. Energy diagram of frontier molecular orbitals for POMo **3** (isovalue = 0.03).

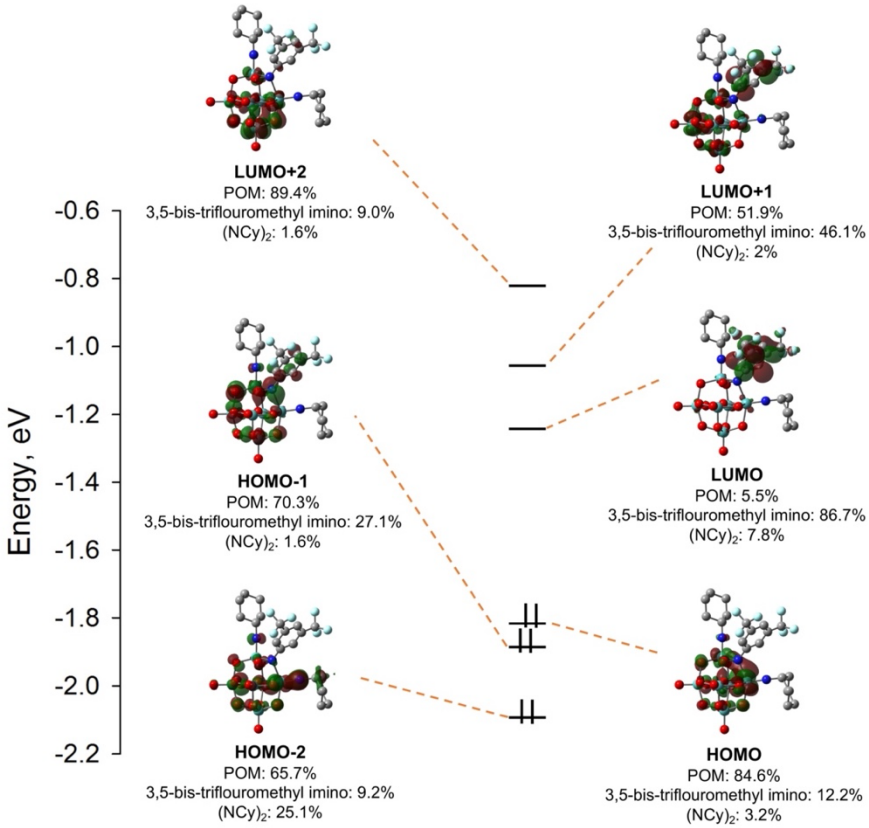

Figure S20. Energy diagram of frontier molecular orbitals for POMo **4** (isovalue = 0.03).

Table S5. Cartesian coordinates for the DFT geometry-optimized species.

Species **1**

Symbol	X	Y	Z
Mo	-0.88999	1.383526	0.144519
Mo	-0.77083	-0.75369	-2.35617
Mo	-0.77494	-3.30959	-0.16641
Mo	-0.88219	-1.06965	2.338697
Mo	1.480236	-0.90861	0.044278
Mo	-3.22542	-0.98774	-0.0715
O	-0.722	-0.8045	-0.00217
O	-0.96162	1.065533	-1.79627
O	-0.68405	-2.66664	-1.97561
O	-0.73515	-2.91336	1.713305
O	-1.0082	0.815706	2.018783
O	1.080179	-0.68714	-1.8701
O	1.139713	-2.76109	-0.10453
O	1.008448	-0.94429	1.925128
O	-2.67238	-0.94333	-1.89886
O	-2.59956	-2.88733	-0.16447
O	-2.87528	0.832322	0.078711
O	-2.73205	-1.18969	1.793826
O	-0.7721	-0.67585	-4.0656
O	-0.70775	-5.01258	-0.27864
O	-0.93325	-1.21845	4.042546
O	-4.9279	-1.126	-0.10732
N	1.084149	1.232988	0.157928
N	-1.09371	3.119697	0.247577
N	3.232188	-0.78896	0.090078
C	2.035648	2.22122	0.225192
C	2.618967	2.657753	1.454335
C	3.592386	3.655172	1.528239
C	3.502946	3.907597	-0.86088
C	2.5299	2.909042	-0.92517
C	-1.36506	4.516384	0.315564
H	-0.43046	5.026271	0.621451
C	-2.45504	4.803519	1.377613
H	-2.14316	4.360277	2.334581
H	-2.514	5.899179	1.520138
C	-3.81961	4.252534	0.945076
H	-3.76135	3.153042	0.892413
H	-4.58004	4.497233	1.705453
C	-4.2376	4.803318	-0.42626
H	-4.39888	5.897092	-0.35082

H	-5.19962	4.361463	-0.7323
C	-3.1663	4.518399	-1.48927
H	-3.08432	3.430666	-1.64158
H	-3.45955	4.954174	-2.45895
C	-1.79636	5.063886	-1.06684
H	-1.83167	6.167793	-1.00117
H	-1.02817	4.799498	-1.80822
C	4.638516	-0.60337	0.145242
H	4.854293	0.235168	0.842116
C	5.331437	-1.86931	0.699215
H	5.058525	-2.71708	0.048939
H	4.924796	-2.09163	1.69632
C	6.856643	-1.70616	0.746088
H	7.117008	-0.91766	1.475579
H	7.323707	-2.63572	1.11267
C	7.428802	-1.32542	-0.62707
H	7.268024	-2.16355	-1.32881
H	8.51994	-1.17366	-0.56075
C	6.744125	-0.06837	-1.1818
H	7.13439	0.169719	-2.18533
H	6.995526	0.793139	-0.537
C	5.219197	-0.23049	-1.23711
H	4.736502	0.690734	-1.59254
H	4.945235	-1.02718	-1.94861
H	3.824841	4.381557	-1.78858
H	3.983937	3.928848	2.508428
C	4.043614	4.285213	0.368318
H	4.80457	5.065566	0.422184
Cl	1.892778	2.497332	-2.49267
Cl	2.086255	1.930814	2.943815

Species **2**

Symbol	X	Y	Z
Mo	-0.34611	-1.65378	0.035833
Mo	-0.42066	1.658642	0.229076
Mo	2.869836	1.785702	0.001288
Mo	1.361774	-0.07599	2.37239
Mo	2.946786	-1.56912	-0.19468
Mo	1.036781	0.179304	-2.33671
O	1.066663	0.044609	0.024576
O	4.062011	3.0057	0.038358
O	1.479162	-0.21385	4.071664
O	4.218699	-2.69629	-0.34516
O	1.002375	0.324388	-4.03946
O	0.036166	-1.47408	1.888661

O	1.358694	-2.62114	-0.22702
O	-0.16008	-1.20221	-1.93778
O	1.197875	2.730016	0.252327
O	2.590199	1.281957	1.907708
O	3.854251	0.149906	-0.07848
O	2.404006	1.565758	-1.79782
O	-0.07665	1.176771	2.092016
O	2.658959	-1.36387	1.698975
O	2.512875	-1.04012	-1.99509
O	-0.23024	1.486558	-1.7169
O	-7.83028	-0.96627	-0.83193
O	-7.90312	0.399407	0.884649
N	-1.63544	-0.05477	0.115231
N	-1.47	-2.99626	-0.00269
N	-1.64905	2.904904	0.324474
N	-7.26465	-0.25901	0.032357
C	-2.99279	-0.09566	0.084394
C	-3.78391	0.631479	1.030253
H	-3.25825	1.210553	1.789187
C	-5.16397	0.569283	1.02099
H	-5.75921	1.100695	1.762495
C	-5.8273	-0.20132	0.04758
C	-5.08322	-0.91604	-0.9099
H	-5.61773	-1.49113	-1.66496
C	-3.70247	-0.87235	-0.88593
H	-3.11502	-1.4069	-1.63205
C	-2.29972	-4.15427	-0.03844
H	-3.35303	-3.8132	-0.07042
C	-2.01137	-4.99529	-1.30642
H	-2.78226	-5.78553	-1.37316
H	-2.11857	-4.35457	-2.19403
C	-0.6133	-5.62466	-1.26066
H	0.141915	-4.82204	-1.28004
H	-0.45016	-6.23846	-2.16203
C	-0.41928	-6.47049	0.005871
H	0.605984	-6.87308	0.036645
H	-1.10214	-7.34227	-0.02413
C	-0.69809	-5.6462	1.270888
H	0.054371	-4.84601	1.354664
H	-0.59585	-6.27451	2.171146
C	-2.09418	-5.01207	1.234633
H	-2.87028	-5.79986	1.242427
H	-2.25628	-4.38043	2.120215
C	-2.6113	3.954999	0.26788

H	-3.59178	3.51934	0.53941
C	-2.70298	4.529617	-1.16277
H	-3.48716	5.307294	-1.15354
H	-3.03853	3.742927	-1.85297
C	-1.35472	5.119444	-1.62857
H	-0.75419	4.329377	-2.09995
H	-1.55237	5.8775	-2.40541
C	-0.55048	5.74386	-0.4639
H	0.133817	4.988168	-0.04622
H	0.083951	6.562717	-0.8384
C	-1.48193	6.250903	0.643327
H	-2.18473	6.991309	0.219305
H	-0.90855	6.781616	1.420132
C	-2.26961	5.09009	1.285768
H	-1.68559	4.640046	2.101115
H	-3.2065	5.466383	1.728488

Species **3**

Symbol	X	Y	Z
Mo	0.293765	1.62761	0.010036
Mo	0.159189	-1.63721	0.384305
Mo	-3.11469	-1.59894	-0.0867
Mo	-1.6821	0.308894	2.291591
Mo	-2.97781	1.74048	-0.46901
Mo	-1.03626	-0.24296	-2.37224
O	-1.21971	0.030301	-0.02161
O	-4.38655	-2.73794	-0.07493
O	-1.88136	0.515984	3.977604
O	-4.16551	2.93863	-0.73197
O	-0.91828	-0.45177	-4.06594
O	-0.19192	1.545693	1.847215
O	-1.3303	2.693737	-0.36811
O	0.173171	1.124666	-1.96324
O	-1.53024	-2.62629	0.27031
O	-2.91444	-1.04113	1.815204
O	-3.99217	0.10049	-0.26851
O	-2.56392	-1.45615	-1.87287
O	-0.28077	-1.08138	2.156658
O	-2.81569	1.609208	1.501585
O	-2.48066	1.124997	-2.17766
O	0.076435	-1.56741	-1.63577
N	1.461857	-0.04258	0.185492
N	1.526767	2.873062	-0.02297
N	1.298135	-2.95254	0.60653
C	2.827157	-0.0965	0.067871

C	3.633546	-0.70889	1.06698
H	3.133105	-1.1374	1.93561
C	5.017327	-0.7397	0.962102
H	5.608544	-1.20202	1.754614
C	5.665207	-0.18586	-0.15589
C	4.885658	0.414669	-1.1598
H	5.372388	0.83626	-2.04101
C	3.502402	0.463501	-1.05216
H	2.895552	0.911	-1.83965
C	2.47434	3.935272	-0.07666
H	3.443856	3.511568	-0.40511
C	2.024547	5.001967	-1.10606
H	2.854403	5.721309	-1.23943
H	1.853784	4.510801	-2.07521
C	0.758517	5.733152	-0.64118
H	-0.07516	5.012951	-0.60441
H	0.480711	6.505151	-1.37801
C	0.953505	6.364169	0.745127
H	0.018904	6.845331	1.076231
H	1.716658	7.164569	0.679321
C	1.402219	5.319573	1.777742
H	0.596117	4.584747	1.931304
H	1.584195	5.798789	2.754247
C	2.664369	4.579569	1.31829
H	3.515243	5.283452	1.255028
H	2.938914	3.795719	2.039262
C	2.178667	-4.07078	0.679376
H	3.171423	-3.6901	0.987843
C	2.319444	-4.75501	-0.69804
H	3.036913	-5.58634	-0.57745
H	2.761832	-4.04995	-1.41559
C	0.963512	-5.27804	-1.21734
H	0.45796	-4.48309	-1.78266
H	1.152804	-6.10362	-1.92467
C	0.039097	-5.75427	-0.07283
H	-0.60897	-4.92131	0.242677
H	-0.63219	-6.54936	-0.4344
C	0.854601	-6.24719	1.129123
H	1.523628	-7.06608	0.805836
H	0.19253	-6.67668	1.898016
C	1.6878	-5.10319	1.745008
H	1.089359	-4.55432	2.485835
H	2.563079	-5.51443	2.275026
C	7.149632	-0.17473	-0.24008

F	7.619053	-0.18402	-1.52806
F	7.728016	0.941826	0.341445
F	7.735747	-1.24257	0.391565

Species **4**

Symbol	X	Y	Z
Mo	0.651606	1.533903	0.076868
Mo	-0.33703	-1.50532	-0.62843
Mo	2.633086	-2.53697	0.237253
Mo	2.192439	-0.25064	-2.2607
Mo	3.79619	0.613217	0.577871
Mo	1.321993	-0.41698	2.529821
O	1.49623	-0.4111	0.128514
O	3.326335	-4.09183	0.37806
O	2.624566	-0.1097	-3.90379
O	5.319609	1.284488	0.950567
O	0.887417	-0.60337	4.176246
O	1.276092	1.309493	-1.78633
O	2.602292	2.033817	0.49606
O	0.60934	1.243539	2.06128
O	0.702675	-2.98624	-0.1357
O	2.822121	-2.05226	-1.55701
O	4.029166	-1.35747	0.708023
O	1.85313	-2.17	2.025681
O	0.448325	-1.12096	-2.28171
O	3.831231	0.361707	-1.26571
O	3.046842	0.23649	2.444897
O	-0.65864	-0.92921	1.452701
N	-1.05994	0.102859	0.522242
N	-0.22168	3.047359	-0.14537
N	-1.88291	-2.19978	-1.10091
C	-2.40052	0.457949	0.678931
C	-3.14429	0.059758	1.805185
H	-2.64811	-0.53674	2.567366
C	-4.48515	0.436622	1.923591
C	-5.119	1.19585	0.937907
H	-6.16488	1.47965	1.036224
C	-4.36997	1.58711	-0.18236
C	-3.03008	1.23712	-0.31656
H	-2.45336	1.54961	-1.18553
C	-5.28051	-0.04364	3.107635
C	-5.05424	2.414901	-1.23475
C	-0.87942	4.279845	-0.43313
H	-1.94488	4.186519	-0.14215
C	-0.2486	5.426062	0.397687
H	-0.87683	6.327472	0.269715

H	-0.27603	5.151315	1.462431
C	1.189345	5.720636	-0.04777
H	1.598709	6.559167	0.540413
H	1.81708	4.842201	0.172007
C	1.259248	6.036741	-1.54908
H	2.306968	6.193275	-1.85367
H	0.726415	6.987402	-1.74852
C	0.629301	4.91499	-2.38805
H	0.641248	5.184073	-3.4574
H	1.22512	3.994201	-2.2868
C	-0.808	4.618781	-1.9425
H	-1.45444	5.497047	-2.12789
H	-1.22205	3.780185	-2.52123
C	-3.13985	-2.79702	-1.38657
H	-3.93738	-2.1964	-0.89719
C	-3.2143	-4.23067	-0.8143
H	-2.38442	-4.81311	-1.24769
H	-3.03853	-4.19241	0.270308
C	-4.55857	-4.89854	-1.13218
H	-5.36748	-4.35705	-0.60924
H	-4.56921	-5.92864	-0.73902
C	-4.84877	-4.8991	-2.63962
H	-4.10512	-5.53711	-3.15006
H	-5.83813	-5.34377	-2.8415
C	-4.77254	-3.4792	-3.21867
H	-4.9366	-3.50053	-4.30893
H	-5.59144	-2.87169	-2.79269
C	-3.42792	-2.80891	-2.90459
H	-3.40365	-1.77714	-3.28446
H	-2.60618	-3.34936	-3.40325
F	-5.81452	-1.29181	2.898393
F	-4.54355	-0.13154	4.244427
F	-6.3449	0.771172	3.390842
F	-4.30053	2.611277	-2.34462
F	-5.39949	3.660576	-0.77044
F	-6.23077	1.844846	-1.65469

References

1. W. G. Klemperer, in *Inorg. Synth.*, ed. A. P. Ginsberg, 1990, vol. 27, ch. 15, pp. 74-85.
2. C. Lv, J. Zhang, J. Hao, L. Liu and Y. Wei, *Dalton Trans.*, 2012, **41**, 10065-10070.
3. T. S. Jadhav, S. A. Abbas, Y.-C. Liu, W.-T. Wu, G.-H. Lee, C.-W. Chu and M.-H. Chiang, *ACS Appl. Energy Mater.*, 2021, **4**, 643-654.
4. C.-C. Lin, C.-T. Hsu, W. Liu, S.-C. Huang, M.-H. Lin, U. Kortz, A. S. Mougharbel, T.-Y. Chen, C.-W. Hu, J.-F. Lee, C.-C. Wang, Y.-F. Liao, L.-J. Li, L. Li, S. Peng, U. Stimming and H.-Y. Chen, *ACS Appl. Mater. Interfaces*, 2020, **12**, 40296-40309.
5. S.-C. Huang, C.-C. Lin, C.-T. Hsu, C.-H. Guo, T.-Y. Chen, Y.-F. Liao and H.-Y. Chen, *J. Mater. Chem. A*, 2020, **8**, 21623-21633.
6. R. N. Nasim Khan, N. Mahmood, C. Lv, G. Sima, J. Zhang, J. Hao, Y. Hou and Y. Wei, *RSC Adv.*, 2014, **4**, 7374-7379.
7. A. M. Zhang, M. Zhang, D. Lan, H.-N. Wang, Y.-J. Tang, X.-L. Wang, L.-Z. Dong, L. Zhang, S.-L. Li and Y.-Q. Lan, *Inorg. Chem.*, 2018, **57**, 11726-11731.
8. H. Hu, Y. Yang, X. Jiang, J. Wang, D. Cao, L. He, W. Chen and Y.-F. Song, *Chem.-Eur. J.*, 2021, **27**, 13367-13375.
9. H. Ilbeygi, S. Kim, I. Y. Kim, S. Joseph, M. G. Kim and A. Vinu, *J. Mater. Chem. A*, 2022, **10**, 12132-12140.
10. J.-N. Chang, M. Zhang, G.-K. Gao, M. Lu, Y.-R. Wang, C. Jiang, S.-L. Li, Y. Chen and Y.-Q. Lan, *Energy Fuels*, 2020, **34**, 16968-16977.
11. J. Wang, Y. Liu, Q. Sha, D. Cao, H. Hu, T. Shen, L. He and Y.-F. Song, *ACS Appl. Mater. Interfaces*, 2022, **14**, 1169-1176.
12. X. Chen, Z. Wang, R. Zhang, L. Xu and D. Sun, *Chem. Commun.*, 2017, **53**, 10560-10563.
13. T. Wei, M. Zhang, P. Wu, Y.-J. Tang, S.-L. Li, F.-C. Shen, X.-L. Wang, X.-P. Zhou and Y.-Q. Lan, *Nano Energy*, 2017, **34**, 205-214.
14. X. Zhao, G. Niu, H. Yang, J. Ma, M. Sun, M. Xu, W. Xiong, T. Yang, L. Chen and C. Wang, *CrystEngComm*, 2020, **22**, 3588-3597.
15. J.-H. Liu, M.-Y. Yu, J. Yang, Y.-Y. Liu and J.-F. Ma, *Micropor. Mesopor. Mat.*, 2021, **310**, 110666.
16. B. Iqbal, X. Jia, H. Hu, L. He, W. Chen and Y.-F. Song, *Inorg. Chem. Front.*, 2020, **7**, 1420-1427.
17. W. Cheng, F.-C. Shen, Y.-s. Xue, X. Luo, M. Fang, Y.-Q. Lan and Y. Xu, *ACS Appl. Energy Mater.*, 2018, **1**, 4931-4938.
18. J. Hu, F. Jia and Y.-F. Song, *Chem. Eng. J.*, 2017, **326**, 273-280.
19. J. Xie, Y. Zhang, Y. Han and C. Li, *ACS Nano*, 2016, **10**, 5304-5313.
20. M.-T. Li, J.-W. Sun, L. Yi Fei, M.-H. Niu, H.-Y. Zou, D.-Q. Sun and Y. Yu, *CrystEngComm*, 2022, **24**, 1279-1284.
21. J. K. Shon, H. S. Lee, G. O. Park, J. Yoon, E. Park, G. S. Park, S. S. Kong, M. Jin, J.-M. Choi, H. Chang, S. Doo, J. M. Kim, W.-S. Yoon, C. Pak, H. Kim and G. D. Stucky, *Nat. Commun.*, 2016, **7**, 11049.
22. A. Bhaskar, M. Deepa and T. Narasinga Rao, *ACS Appl. Mater. Interfaces*, 2013, **5**, 2555-2566.
23. Y. Wang, H. Zhao, A. Di, X. Yang, B. Cong and G. Chen, *Int. J. Energy Res.*, 2021, **45**, 9438-9448.
24. J. Yu, M.-L. Wang, Z.-X. Yang, K. Li, X.-P. Yang, G.-G. Gao, D. Yin, L.-L. Fan and H. Liu, *Dalton Trans.*, 2021, **50**, 14595-14601.
25. Q. Tang, Z. Shan, L. Wang and X. Qin, *Electrochim. Acta*, 2012, **79**, 148-153.

26. S. B. Patil, Udayabhanu, B. Kishore, G. Nagaraju and J. Dupont, *New J. Chem.*, 2018, **42**, 18569-18577.